Statistical signatures of critical behavior in small systems

J. B. Elliott,[1] S. Albergo,[2] F. Bieser,[6] F. P. Brady,[3] Z. Caccia,[2] D. A. Cebra,[3] A. D. Chacon,[7] J. L. Chance,[3] Y. Choi,[1]
S. Costa,[2] M. L. Gilkes,[1] J. A. Hauger,[1] A. S. Hirsch,[1] E. L. Hjort,[1] A. Insolia,[2] M. Justice,[5] D. Keane,[5] J. C. Kintner,[3]
V. Lindenstruth,[4] M. A. Lisa,[6] H. S. Matis,[6] M. McMahan,[6] C. McParland,[6] W. F. J. Müller,[4] D. L. Olson,[6]
M. D. Partlan,[3] N. T. Porile,[1] R. Potenza,[2] G. Rai,[6] J. Rasmussen,[6] H. G. Ritter,[6] J. Romanski,[2] J. L. Romero,[3] G. V. Russo,[2]
H. Sann,[4] R. P. Scharenberg,[1] A. Scott,[5] Y. Shao,[5] B. K. Srivastava,[1] T. J. M. Symons,[6] M. Tincknell,[1] C. Tuvé,[2]
S. Wang,[5] P. G. Warren,[1] H. H. Wieman,[6] T. Wienold,[6] and K. Wolf[7]

(EOS Collaboration)

[1]*Purdue University, West Lafayette, Indiana 47907*
[2]*Universitá di Catania and Istituto Nazionale di Fisica Nucleare-Sezione di Catania, I-95129 Catania, Italy*
[3]*University of California, Davis, California 95616*
[4]*GSI, D-64220 Darmstadt, Germany*
[5]*Kent State University, Kent, Ohio 44242*
[6]*Nuclear Science Division, Lawrence Berkeley National Laboratory, Berkeley, California 94720*
[7]*Texas A&M University, College Station, Texas 77843*
(Received 9 February 2000; published 30 October 2000)

The cluster distributions of three different systems are examined to search for signatures of a continuous phase transition. In a system known to possess such a phase transition, both sensitive and insensitive signatures are present; while in systems known not to possess such a phase transition, only insensitive signatures are present. It is shown that nuclear multifragmentation results in cluster distributions belonging to the former category, suggesting that the fragments are the result of a continuous phase transition.

PACS number(s): 25.70.Pq, 64.60.Ak, 24.60.Ky, 05.70.Jk

I. INTRODUCTION

Multifragmentation, the breakup of a system into several intermediate sized pieces, is of great interest in many areas of physics. Several recent works have been presented on a variety of systems including fullerene's [1–3] as well as the fragmentation of collisions in solids [4]. This work examines the breakup of excited nuclei, nuclear multifragmentation.

Beginning in the 1970's significant advances in the understanding of nuclear multifragmentation were made possible with the advent of high statistics inclusive experiments. Typically, only one intermediate mass fragment ($3 \leq Z_f \leq 30$) was detected per event. From these inclusive studies came the first evidence that intermediate mass fragments (IMFs) were associated with a simultaneous multibody breakup of a system which had undergone expansion. A study of the fragment mass yield distribution obtained in an inclusive gas jet experiment conducted at Fermilab contained the first indication that nuclear multifragmentation might be related to critical phenomena normally observed in macroscopic systems [5]. The Purdue Group was the first to make the suggestion that the observed power law in the fragment yield distribution might result from a system whose excitation energy was comparable to its total binding energy [6]. The exponent of the power law was $2 \leq \tau \leq 3$, within the range expected for a system near its critical point.

The presence of the power law and the value of the exponent, coupled with the strong similarity of the nuclear and van der Waals potentials, led the Purdue group to suggest that multifragmentation of nuclei might be analogous to a fluid undergoing a continuous phase transition from a liquid to a gas. Furthermore, the Fisher droplet model (FMD)

[7–10], used to describe condensation in a fluid system near its critical point, after modification for nuclear physics effects, was capable of describing the isotopic yields of 50 fragments with one set of parameters [6,11]. The temperature of the system was determined to be about 5 MeV [6], a reasonable value considering that the average binding energy per nucleon in a nucleus is approximately 8 MeV. The success of this approach reinforced the notion that multifragmentation was both a thermal process and that it was related to critical phenomena.

With the advent of exclusive experiments capable of detecting all of the charged reaction products, the possibility of studying multifragmentation on an event-by-event basis became a reality. High statistics exclusive experiments in which the fragmenting system is characterized according to its nucleon number and excitation energy permit both the correlation of dynamical and statistical information and the study of fluctuations in experimental observables. Fluctuations are central to all critical phenomena, and indeed, such fluctuations are apparent in exclusive multifragmentation data. In this paper, the focus will be on the statistical signals of multifragmentation data observed in the EOS experiment [12–14]. Comparisons will be made with two other systems, one of which exhibits critical behavior and one of which does not.

Much of the pioneering work in understanding the statistical aspects of multifragmentation was performed by Campi [15–22] and Mekjian [23–29]. Both compared multifragmentation data to model systems in order to gain some insight into the nuclear breakup process. In this paper, many of the ideas suggested by these authors are followed and applied to the EOS data and the model systems in order to

demonstrate which signals are most useful in the identification of critical behavior. Several methods proposed for detecting signals of critical phenomena in multifragmentation are reviewed in this paper.

It is tempting to compare the experimental data to dynamical models that attempt to describe nuclear multifragmentation. However, the task of modeling multifragmentation from the initial collision phase of the reaction to freeze-out has proven to be a daunting task. Models that adequately describe the initial stage of the reaction [30–35] do not satisfactorily describe the fragment formation stage, in either statistical or dynamical aspects. Likewise, the most successful models in describing the statistical properties of nuclear multifragmentation [36–41], assume thermodynamic equilibrium, yet fail to adequately match the dynamical features of the data.

Molecular dynamical approaches, which have enjoyed considerable success in describing critical behavior in classical systems [42–46], have not been conclusive in describing nuclear multifragmentation and at times have yielded contradictory results. Later studies suggested flaws in the application of molecular dynamical models to nuclear multifragmentation, therefore calling into question the conclusions drawn from the earlier studies [47].

The most striking of the early theoretical efforts came from Campi's analysis of a few hundred completely reconstructed emulsion multifragmentation events [48] and the comparison of these data to clusters generated from a percolation calculation [15,16]. In this series of papers it was shown that the fragment distributions from multifragmentation bore a striking similarity to the cluster distributions from percolation lattices. This analysis provided strong evidence that multifragmentation was a statistical process which appeared to be related to critical phenomena. In that analysis another estimate of the exponent τ was made which agreed with the first measurements from the Purdue Group and several later analyses of various fragment distributions.

In the early 1990's the ALADIN Group from GSI performed several multifragmentation experiments [49–51]. Of particular importance was the "rise and fall" of multifragmentation. In one analysis the ALADIN group plotted the "rise and fall" curve of the production of IMFs versus an observable related to the excitation energy of the reaction for several multifragmenting systems. With the appropriate scaling the data collapsed to a single curve suggesting that the multifragmenting systems retained no memory of the reaction entrance channel. This is expected for an equilibrated system.

However, other statistical analyses of multifragmentation data yielded results that could be interpreted to suggest that multifragmentation is a sequential decay [52–54] in contrast to the phase transition picture. The same sort of statistical analysis has also been applied to explicitly simultaneous models [47] and produced results that were similar to those of multifragmentation data. Thus those signals could be interpreted as evidence for either sequential or simultaneous multifragmentation [54].

This last effort puts into focus the main question in this work: what type of analysis of the statistical aspects of a cluster distribution can provide the most insight into the nature of the mechanism which created the clusters? Specifically, can those systems which contain critical behavior be distinguished from those which do not? It will be argued that this question has two answers. Analysis of the *insensitive* features of the cluster distribution cannot make the above-mentioned distinction [55]. However, an analysis of the *sensitive* features of the cluster distribution will be shown to provide deeper insight into the cluster production mechanism. A similar type of analysis has been previously reported for clusters resulting from nuclear multifragmentation [12–14] and have been performed on models [56,57]. Note that the more generic term ''cluster'' will be used to refer to any composite of constituents, whether these be molecules of a fluid, nuclear fragments or percolation clusters.

The method employed to address the above question is as follows. The same analysis is performed on the cluster distributions produced by three different systems. In one case, clusters are generated by randomly partitioning an integer. Such one-dimensional partitioning does not posses critical behavior indicative of a continuous phase transition. In the second case, three-dimensional bond building percolation is used to produce clusters. Percolation is well-known mathematical construct that possesses a continuous phase transition, i.e., a critical point. Finally, the cluster distributions resulting from the multifragmentation of gold nuclei are analyzed. Although it is not known, *a priori*, whether the nuclear multifragmentation bears any relation to critical phenomena, it will be seen that the analysis presented in this work yields suggestive results.

This paper is organized as follows. In Sec. II a brief description of each system is presented. In Sec. III the Fisher droplet model is reviewed; this section may be omitted by readers already familiar with the model. In Sec. IV A the insensitive signatures of the cluster distributions for all systems are examined. In Sec. IV B the sensitive signatures are examined. Sections V and VI present possible corrections to the analysis of the multifragmentation data. Finally, Sec. VII discusses the conclusions reached upon the completion of the analyses in Secs. IV and V. Throughout this paper the term ''continuous phase transition'' will be used instead of ''second order phase transition,'' the latter from the outdated Ehrenfest theory of phase transitions [58].

II. DESCRIPTION OF SYSTEMS UNDER STUDY

A. 1.0A GeV Au + C multifragmentation

Approximately 40 000 fully reconstructed events ($76 \leq Z_{observed} \leq 82$) were collected with the EOS experimental apparatus discussed in Ref. [12]. In the collision of the projectile gold nucleus (197, 79) and the target carbon nucleus, so-called prompt nucleons are knocked out of the gold nucleus by quasielastic and inelastic collisions between projectile and target nucleons [59]. Immediately following the collision, the gold projectile remnant is in an excited state with fewer than 197 nucleons. The excited remnant cools and expands and may evolve to the neighborhood of the

critical point in the temperature-density plane [60], where clusters condense from a high temperature low density vapor of nucleons.

The charge and mass of the projectile remnant, Z_0 and A_0, were determined for each event by subtracting the charge and mass of the prompt particles from the charge and mass of the gold nucleus [60]. Prompt particles have $Z_f = 0$, 1, and 2 and were removed from the cluster distributions analyzed in this work. Only clusters created from the excited gold projectile were considered in the ensuing analysis. For events with the lowest total charged particle multiplicities m, the remnant had $Z_0 \sim 76$, $A_0 \sim 194$, and $E^*/A_0 \sim 2$ MeV/nucleon, while for events with the highest multiplicities the remnant had $Z_0 \sim 39$, $A_0 \sim 92$, and $E^*/A_0 \sim 16$ MeV/nucleon [60].

Clusters of a given charge Z_f were counted on an event by event basis to determine the cluster charge distribution N_{Z_f}. In this analysis, although the mass number of the clusters was of interest, a cluster's charge was used as an index. Mass numbers for clusters of charge 1 and 2 were measured in the EOS time projection chamber. Clusters with $Z_f \geqslant 3$ were assigned a mass number A_f by multiplying the cluster charge by the mass to charge ratio of the excited gold projectile remnant; for low m events $A_0/Z_0 \sim 2.55$ and for high m events $A_0/Z_0 \sim 2.36$. This procedure provided an estimate of a cluster's mass number prior to any secondary decay effects. It was assumed that on average $N_{A_f} = N_{Z_f}$. The normalized cluster distribution $n_{A_f} = N_{A_f}/A_0(m)$ was used in the analysis presented in this paper.

B. Percolation

Bond building percolation calculations were performed on three-dimensional simple cubic lattices of 216 sites. Cluster distributions for 100 000 lattice realizations were generated in the standard fashion by forming bonds between sites. Bonds were either active (on) or inactive (off) according to the following algorithm.

The control parameter (e.g., temperature in thermodynamic systems) for percolation is the lattice probability p_l. A single value of p_l was chosen for the entire lattice. All probabilities were between 0 and 1. Next, a bond probability p_{b_i} was randomly chosen from a uniform distribution on (0,1) for the ith bond. If p_{b_i} was less than p_l, then the ith bond was active and two sites were joined into a cluster. This process was performed for each bond in the lattice.

At low values of p_l, few bonds were formed resulting in a high multiplicity m of small clusters, a distribution analogous to the gaseous phase of a fluid. At high values of p_l, many bonds were formed resulting in a low multiplicity of mostly large clusters, analogous to the liquid phase of a fluid. In an infinite lattice the phase transition occurs at a unique value of the lattice probability, p_c, when the probability of forming a percolating cluster changes from zero to unity [61–63].

To examine the behavior of the average cluster distribution, the number of clusters of size A_f per lattice site was calculated by histogramming the 100 000 lattice realizations

into 100 bins from 0 to 1. The use of m as a control parameter and the ensuing effects on signatures of continuous phase transition were investigated by calculating the average number of clusters of size A_f with the 100 000 lattice realizations histogrammed in units of m.

C. Random partitions

Random partitions were generated from 79 total system constituents, chosen to approximate the number of charges in the gold multifragmentation system. The algorithm is as follows. First a random choice of m was made from a uniform distribution on (1,79). Next the maximum size of a cluster A_{max}^1 for an event with m was determined; this depended on the constraints of the system size $A_0 = 79$ and the choice of m. The size of the first cluster A_1 was then randomly chosen from a uniform distribution on $(1, A_{max}^1)$. There were then $m - 1$ clusters to be generated from $79 - A_1$ constituents. The maximum size of a cluster for an $m - 1$ event from a 79 $- 1$ constituent system was determined: A_{max}^2. The size of the second cluster A_2 was then randomly chosen form a uniform distribution on $(1, A_{max}^2)$. This process was repeated until all constituents belonged to a cluster. 100 000 partitions were generated in this manner. This particular weighting results in a power law cluster distribution [26].

III. REVIEW OF THE FISHER DROPLET MODEL

The focus of most studies of phase transitions is on standard thermodynamical variables such as a system's temperature, density, compressibility, etc. These quantities are difficult or impossible to measure directly in present nuclear multifragmentation experiments. Thus a theory which addresses quantities accessible to MF experiments is needed. To that end Fisher's gas-to-liquid phase transition model, based on Mayer's condensation theory, is followed [7,9,61].

Fisher begins his model, called the Fisher droplet model (FDM) hereafter, by writing the free energy for the formation of clusters of size A_f as

$$\Delta G_{A_f} = -k_b T A_f \ln[g(\mu, T)] - k_b T \ln[f(A_f, T)] + k_b T \tau \ln(A_f) + \cdots, \quad (1)$$

where k_b is the Boltzmann constant and the g term is the bulk formation energy, or volume term and

$$g(\mu, T) = \exp[(\mu - \mu_{coex})/k_b T], \quad (2)$$

where μ is the chemical potential and μ_{coex} is the chemical potential along the coexistence curve.

The f term is related to the surface free energy of cluster formation. It is a form given by Fisher

$$f(A_f, T) = \exp[a_0 \omega A_f^\sigma \epsilon T_c/k_b T], \quad (3)$$

where σ is a critical exponent and is related to the ratio of the dimensionality of the surface to the dimensionality of the volume, a_0 is a constant of proportionality relating the average surface area of a droplet to its number of constituents,

and ω is the surface entropy density; ϵ is a measure of the distance from the critical point. For usual thermodynamic systems $\epsilon=(T_c-T)/T_c$, in the percolation treatment $\epsilon=(p_l-p_c)/p_c$ and for multifragmentation $\epsilon=(m_c-m)/m_c$ will be used. All formulations of ϵ are such that $\epsilon>0$ ($\epsilon<0$) corresponds to the liquid (gas) region. This form of the surface free energy is applicable on only one side of the critical point, the single phase side. A more general form suggested by efforts from percolation theory [63–66] that can be applied on both sides of the critical point and leads to a power law which describes the behavior of the order parameter is

$$f(z)=A \exp[-(z-B)^2/C], \tag{4}$$

where the scaling variable z is

$$z=A_f^\sigma\epsilon. \tag{5}$$

The physical interpretation of the parameters A, B, and C is an open question.

Finally τ is another critical exponent depending principally on the dimensionality of the system and has its origins in considerations of a three dimensional random walk of a surface closing on itself, thus for three dimensions $2\leqslant\tau\leqslant3$ [67]. In Eq. (1), q_0 is a normalization constant which will be shown to depend solely on the value of τ [68].

From the free energy of cluster formation the average cluster distribution normalized to the size of the system is

$$n_{A_f}(\epsilon)=\exp(-\Delta G_{A_f}/k_bT)=q_0A_f^{-\tau}f(z)g(\mu,T)^{A_f}. \tag{6}$$

At the critical point $\epsilon=0$ both f and g are unity and the cluster distribution is given by a pure power law

$$n_{A_f}(\epsilon)=q_0A_f^{-\tau}. \tag{7}$$

If the first moment of the normalized cluster distribution is considered at the critical point then [68]

$$M_1(\epsilon=0)=\sum\nolimits_{A_f}n_{A_f}(\epsilon)A_f=q_0\sum\nolimits_{A_f}A_f^{1-\tau}=1.0 \tag{8}$$

when the sum runs over all clusters. From Eq. (8) it is obvious that the value of the overall cluster distribution normalization constant, q_0, is dependent on τ via a Riemann ζ function

$$q_0=1.0/\sum\nolimits_{A_f}A_f^{1-\tau}. \tag{9}$$

The above is true only if the scaling assumptions in the FDM apply to all clusters. For finite size systems even at the critical point this is only approximately true. However, it will be seen that Eq. (9) holds reasonably well at the critical point for systems with a continuous phase transition over some range in cluster size.

In the FDM it is assumed that all clusters of size A_f can be treated as an ideal gas, so that the total pressure of the entire cluster distribution can be determined by summing all of the partial pressures:

$$P/(k_bT)=\sum\nolimits_{A_f}n_{A_f}(\epsilon)=q_0\sum\nolimits_{A_f}A_f^{-\tau}f(z)g(\mu,T)^{A_f}$$
$$=M_0(\epsilon). \tag{10}$$

It is clear from Eq. (10) that the pressure of the system is related to the zeroth moment of the cluster distribution.

The density is then

$$\rho=\frac{\partial P}{\partial\mu}=q_0\sum\nolimits_{A_f}A_f^{1-\tau}f(z)g(\mu,T)^{A_f}$$
$$=\sum\nolimits_{A_f}n_{A_f}(\epsilon)A_f=M_1(\epsilon). \tag{11}$$

The density is given by the first moment of the cluster distribution.

It is now a simple matter to derive the power law which describes the divergence of the isothermal compressibility κ_T. By definition:

$$\kappa_T=-\frac{1}{V}\left(\frac{\partial V}{\partial P}\right)_T=\frac{1}{\rho}\left(\frac{\partial\rho}{\partial P}\right)_T. \tag{12}$$

Noting that $k_bT\rho=g(\mu,T)[\partial P/\partial g(\mu,T)]$, Eq. (12) can be rewritten as

$$\kappa_T=\frac{-1}{\rho^2}\left(g(\mu,T)\frac{\partial P}{\partial g(\mu,T)}+g(\mu,T)^2\frac{\partial^2 P}{\partial g(\mu,T)^2}\right)_T, \tag{13}$$

which leads to

$$\kappa_T=(\rho k_bT)^{-1}+(\rho^2 k_bT)^{-1}\sum\nolimits_{A_f}n_{A_f}(\epsilon)A_f^2$$
$$=(\rho k_bT)^{-1}+(\rho^2 k_bT)^{-1}M_2(\epsilon). \tag{14}$$

The sum in the second term illustrates the relation of the second moment of the cluster distribution $M_2(\epsilon)$ to the isothermal compressibility. The sums in Eqs. (10), (11), and (14) run over all clusters in the gas and exclude the bulk liquid drop. In percolation and multifragmentation the largest cluster on the liquid side of the critical point will be considered as the liquid drop and will thus be excluded from the sum. On the gas side of the critical point, the sum runs over all clusters as there is no longer a liquid drop.

In the thermodynamic limit, large A_f dominate the sum so that it may be treated as an integral giving

$$\kappa_T=(\rho k_bT)^{-1}+(\rho^2 k_bT)^{-1}\int_0^\infty n_{A_f}(\epsilon)A_f^2 dA_f. \tag{15}$$

Working along the liquid-gas coexistence curve so that $g(\mu,T)=1$ Eq. (15) reduces to

$$\kappa_T=(\rho k_bT)^{-1}+(\rho^2 k_bT)^{-1}\int_0^\infty A_f^{2-\tau}f(z)dA_f. \tag{16}$$

A change of variables from A_f to z shows that near the critical point

$$\kappa_T \sim (\rho^2 k_b T)^{-1} \left| \frac{q_0}{\sigma} \int_0^{\pm\infty} dz f(z) |z|^{(3-\tau-\sigma)/\sigma} \right| |\epsilon|^{(\tau-3)/\sigma}$$

$$= (\rho^2 k_b T)^{-1} \Gamma_\pm |\epsilon|^{-\gamma}. \tag{17}$$

This is the so-called γ-power law which describes the divergence of the isothermal compressibility and the second moment of the cluster distribution near the critical point. The scaling relation between the exponents γ, σ, and τ is

$$\gamma = \frac{3-\tau}{\sigma}. \tag{18}$$

The absolute normalization constants of the $M_2(\epsilon)$ power law depend on the scaling function $f(z)$ the exponent σ and the overall normalization of the cluster distribution q_0 which in turn depends on the exponent τ

$$\Gamma_\pm = \left| \frac{q_0}{\sigma} \int_0^{\pm\infty} dz \, f(z) |z|^{(3-\tau-\sigma)/\sigma} \right|. \tag{19}$$

The second moment is related to the isothermal compressibility by the temperature and density of the system.

The derivation of the γ-power law demonstrates one way to arrive at the scaling relations between the critical exponents. In addition it illustrates the existence of only two independent exponents and shows the relation of the moments of the cluster distribution to familiar thermodynamic quantities. Fisher's framework here illustrated and tempered by percolation theory will be used in the analysis of the cluster distributions of the three systems discussed above. It will be seen that in the case of systems which exhibit a continuous phase transition, the framework of Fisher is well followed, while for systems with no such phase transition, the framework fails, as it should.

IV. PHASE TRANSITION SIGNATURES IN CLUSTER DISTRIBUTIONS

A. Insensitive signatures

In this section the insensitive features of the cluster distribution for each system are examined. It will be demonstrated that on the level of analysis presented here, each system exhibits behaviors that are consistent with systems which undergo a continuous phase transition. The conclusion is inescapable that this sort of analysis can yield necessary, but not sufficient, signals. A deeper analysis will be necessary to distinguish those systems which undergo such a phase transition from those which do not.

1. Fluctuations

One of the most striking characteristics of systems undergoing continuous phase transitions is the occurrence of fluctuations that exist on all length scales in a small range of the control parameter. In fluid systems this was observed as critical opalescence, first noted by Andrews in the latter half of the 19th century [58,69]. Fluctuations in cluster size and the density of the system arise because of the disappearance of the latent heat at the critical point. This is illustrated in the FDM when the isothermal compressibility diverges at the critical point and small changes in pressure gives rise to great changes in the density. In the FDM as the volume and surface contribution to the free energy of cluster formation vanishes the power law dominates and clusters of all length scales are observed [7].

In a cluster distribution the most readily observed fluctuations are those in the size of the largest cluster. For each system the root mean square (rms) fluctuations in the size of the largest cluster normalized to the size of the system $\Delta(A_{max}/A_0)$, have been calculated as a function of the system's control parameter. This measure of the fluctuations in the cluster distribution was first studied by Campi for gold multifragmentation and percolation [16]. Those results are replicated here for those two systems.

Figure 1(a) shows $\Delta(A_{max}/A_0)$, as a function of p_l for percolation. As expected for a system known to exhibit a continuous phase transition, the rms fluctuations peak over a narrow range in the control parameter. The location of this peak provides a first estimate of the critical point; $p_c = 0.33 \pm 0.01$, see Table I.

Next the percolation lattice is examined using the multiplicity of clusters m as an estimate of the control parameter. This is done because in the case of nuclear multifragmentation m is experimentally measurable. Figure 1(b) shows much the same qualitative behavior as Fig. 1(a). The fluctuations peak over some narrow range of m and suggest the value of the multiplicity at the critical point, the *critical multiplicity*, to be $m_c = 55 \pm 5$.

For random partitions a peaking behavior in the fluctuations of the size of the largest cluster as a function of m was observed, see Fig. 1(c). These fluctuations can be understood as follows. At $m = 1$ there can be no fluctuations in the size of the largest cluster because of the dual constraints of event cluster multiplicity and the fixed number of constituents. As the multiplicity increases from unity, the constraints ease and fluctuations in the size of the largest cluster grow. At the maximum possible multiplicity, i.e., when m is equal to the total number of constituents, the size of the largest cluster is constrained to be equal to unity and the fluctuations vanish. Thus, the fluctuations show a peak, but for reasons that have nothing to do with a continuous phase transition. Therefore it must be concluded that the observation of a maximum in the fluctuations of the size of the largest cluster is not sufficient to distinguish systems with and without critical behavior. On the other hand, the absence of a peak in the fluctuations would indicate that the clusters of the system were not produced near a critical point. If the system's phase space has been fully explored, then the stronger statement that the system does not possess a critical point could be made. At this level of analysis the critical multiplicity of this system can be estimated to be $m_c = 5 \pm 2$.

Finally, Fig. 1(d) shows the Au + C multifragmentation data with the cluster distribution normalized to the size of the system $A_0(m)$. The fluctuations in the mass of the largest cluster exhibit a peak when plotted as a function of the event
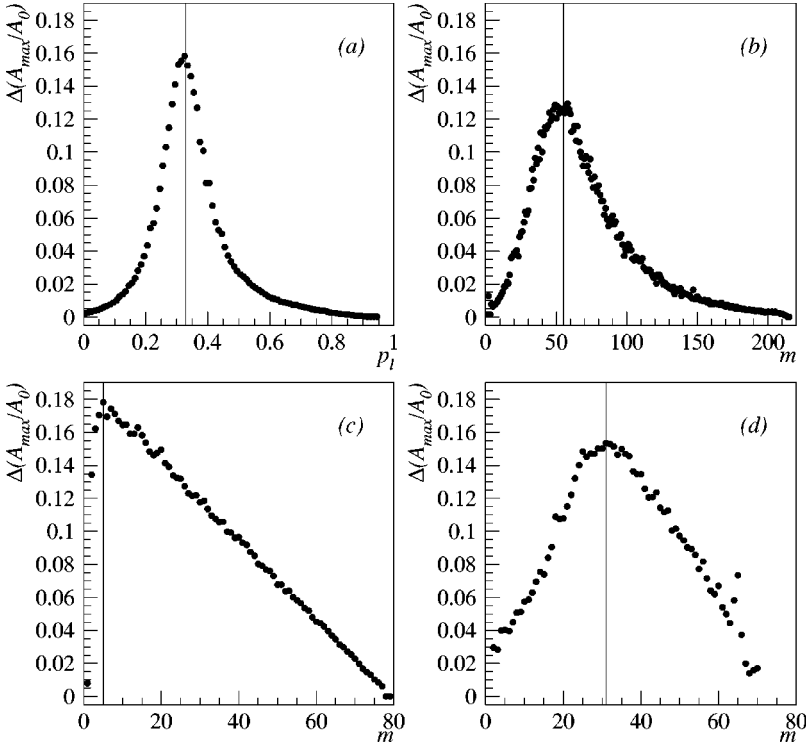
FIG. 1. Fluctuations in the normalized size of the largest cluster for. (a) percolation ($A_0 = 216$) as a function of p_l, (b) percolation as a function of m, (c) random partitions as a function of m, and (d) Au + C multifragmentation as a function of m. Solid vertical lines indicate the guess for the critical point.

total charged particle multiplicity m. This behavior is consistent with what is expected for a critical phenomenon. However, as illustrated above, it is inconclusive. At this level of analysis the estimate for the critical multiplicity is $m_c = 31 \pm 6$.

It is also possible to study the fluctuations in the average size of a cluster. From the example of critical opalescence it is clear that the greatest fluctuations in cluster size should occur at the critical point. To that end the quantity known as γ_2 is constructed, again following the work of Campi [16–21]. The variance in the mean cluster size $\langle A_f \rangle$ is defined as

$$\sigma^2 = \lim_{N \to \infty} \left(\frac{1}{N} \sum A_f^2 \right) - \langle A_f \rangle^2. \tag{20}$$

The average cluster size is given by the ratio of the first moment to the zeroth moment

$$\langle A_f \rangle = \sum n_{A_f} A_f / \sum n_{A_f} = M_1 / M_0. \tag{21}$$

The first term in Eq. (20) is just the ratio of the second moment to the zeroth moment. Therefore, the variance in the average cluster size can be written in terms of the kth moments:

$$\sigma^2 = \frac{M_2}{M_0} - \left(\frac{M_1}{M_0} \right)^2. \tag{22}$$

This quantity is directly related to Campi's γ_2 via

$$\gamma_2 = \frac{\sigma^2}{\langle A \rangle^2} + 1 = \frac{M_2 M_0}{M_1^2}, \tag{23}$$

which is easily measured and was coined by Campi as the reduced variance [16].

In a later paper [20] Campi discussed the differences in methods to measure γ_2. Specifically, the manner in which the kth moments are computed from the observed cluster distribution. One method is to measure the kth-moments on an event by event basis and then compute an average based on the control parameter, e.g.,

TABLE I. Critical point determination.

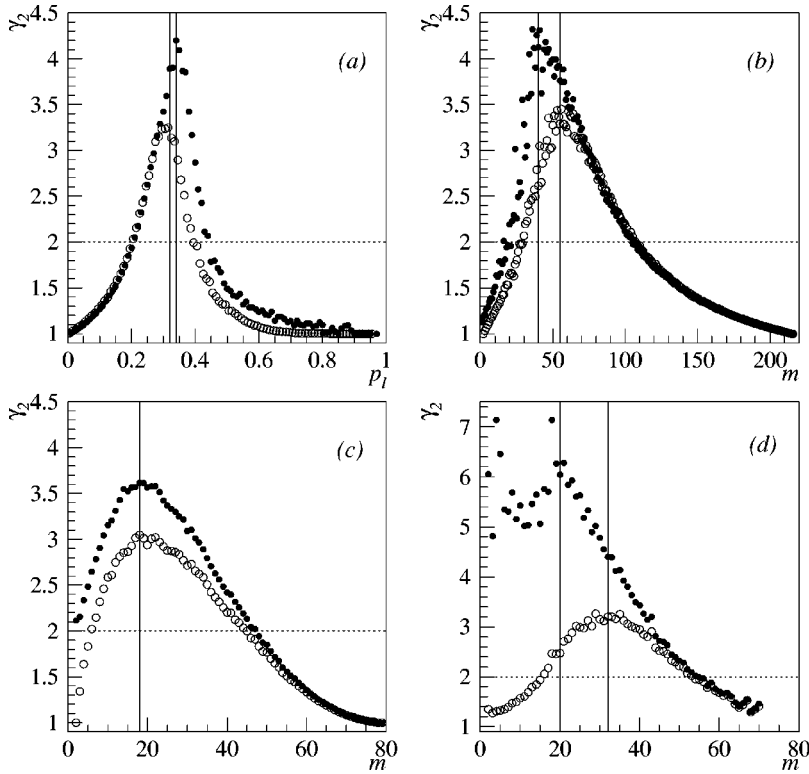| Method/system	Percolation (p_l)	Percolation (m)	Random partitions	Au + C
$\Delta(A_{max}/A_0)$	0.33 ± 0.01	55 ± 5	5 ± 2	31 ± 6
M_2 peak	0.28 ± 0.03	62 ± 2	5 ± 2	35 ± 2
Fisher τ-power law	0.31 ± 0.05	57 ± 3	59 ± 1	22 ± 1
Scaling function	0.34 ± 0.03	57 ± 6	10 ± 2	22 ± 2
γ-matching	0.33 ± 0.02	49 ± 1	9 ± 1	21 ± 2

FIG. 2. Fluctuations as measured by γ_2 for (a) percolation as a function of p_l, (b) percolation as a function of m, (c) random partitions as a function of m, and (d) Au + C multifragmentation as a function of m (at low m $\bar{\gamma}_2$ is affected by fission events not completely filtered). Open circles show $\langle \gamma_2 \rangle$, while filled circles show $\bar{\gamma}_2$ (see text for details). Solid vertical lines indicate the guess for the critical point. A dotted horizontal line shows the value of $\gamma_2 = 2$.

$$\langle M_k(\epsilon) \rangle = \frac{1}{N} \sum_{i=1}^{N} M_k^i(\epsilon) = \frac{1}{N} \sum_{i=1}^{N} \left(\sum_{A_f} n_{A_f}^i(\epsilon) A_f^k \right), \tag{24}$$

where N is the number of events at a control parameter value of ϵ, and i denotes the ith event. This method of calculation of the kth moments will be termed *averaging the sums* and will yield $\langle \gamma_2 \rangle$.

The alternate method involves calculating an average cluster distribution at each value of the control parameter and then calculating the kth moments from the resulting average cluster distribution

$$\bar{M}_k = \sum_{A_f} \langle n_{A_f}(\epsilon) \rangle A_f^k = \sum_{A_f} \left(\frac{1}{N} \sum_{i=1}^{N} n_{A_f}^i(\epsilon) \right) A_f^k. \tag{25}$$

This method of calculation will be termed ''summing the averages'' and will give $\bar{\gamma}_2$.

For quantities linear in n_{A_f} there is no difference in the two methods so that $\langle M_k(\epsilon) \rangle = \bar{M}_k(\epsilon)$. However, due to the dependence of γ_2 on the square of the first moment, there will be a difference in the two methods of calculation. Results for both methods for each system are shown in Fig. 2.

Of primary significance is the presence of a peak in both measurements of γ_2 for all systems. For an infinite system exhibiting critical phenomena, the location of the peak in γ_2 will coincide with the location of the critical point. For the percolation system Figs. 2(a) and 2(b) show that both the location and magnitude of the peak in γ_2 is dependent on the choice of calculation method. Solid lines indicate this measure of the critical point. For the random partitions, Fig. 2(c),

the location of the peak in γ_2 shows little dependence on the method of calculation while the magnitude of the peak does. The gold multifragmentation data exhibit a dependence on the method of calculation both in the magnitude and location of a peak in γ_2.

Having noted the peaking behavior of γ_2, the significance of the amplitude of the peak is now addressed. It has been suggested that the height of the peak can be used to differentiate between the presence of a power law and that of an exponential: for a power law $\gamma_2 > 2$ while for an exponential $\gamma_2 < 2$. This alone is not definitive proof of the existence of a continuous phase transition as other systems show power laws in the absence of such a phase transition. All of the percolation figures show peaks above two, as do the multifragmentation data plots and the random partitions. However, the value of γ_2 depends on the size of the system in question [20]. For a percolation system with 64 sites, peaks in γ_2 under two are observed, see Figs. 3(a) and 3(c). Therefore, the lone criterion $\gamma_2 > 2$ is not sufficient to discriminate between those finite systems which do and those which do not posses a power law cluster distribution.

Finally the question of the difference between the alternative methods of calculating γ_2 is examined via $\Delta \gamma_2 = \bar{\gamma}_2 - \langle \gamma_2 \rangle$. It has been suggested that a peak in the difference could indicate critical phenomena and the location of the critical point [20]. Unfortunately, the cause of this peak is not well understood and vanishes at the limits of the system size: $(0, \infty)$. Figures 4(a) and 4(b) do show peaks in $\Delta \gamma_2$ at some intermediate value of the control parameter for this percolation lattice of 216 sites. However, as the size of the percolation lattice increases this signal vanishes [20]. For a percolation lattice with 64 sites Figs. 3(c) and 3(d), respec-
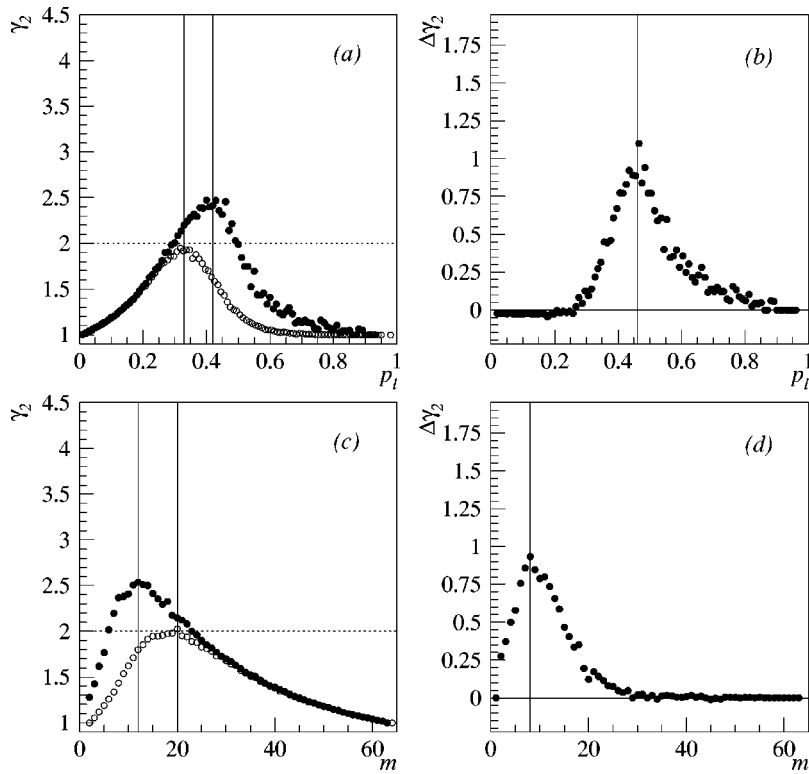
FIG. 3. Fluctuations as measured by γ_2 (see text for details) for a percolation lattice of 64 sites: (a) open circles $\langle \gamma_2 \rangle$, filled circles $\bar{\gamma}_2$ as a function of p_l, (b) $\Delta \gamma_2$ as a function of p_l, (c) open circles $\langle \gamma_2 \rangle$, filled circles $\bar{\gamma}_2$ as a function of m, and (d) $\Delta \gamma_2$ as a function of m. Solid vertical lines indicate the guess for the critical point. A dotted horizontal line shows the value of $\gamma_2 = 2$.

tively, look similar to a cross between the percolation ($L = 6$, m) results, Figs. 2(b) and 4(b), and the random partition results shown in Figs. 2(c) and 4(c). This is believed to be due to the twin constraints of the multiplicity and the conservation of constituents imposed upon the system at the extremes in cluster multiplicity. Similar behavior is observed

in the gold multifragmentation data in Figs. 2(d) and 4(d).

Neither the γ_2 measure of fluctuations nor the observation of fluctuations in the size of the largest cluster provide definitive insight into the nature of the cluster producing mechanism. For a large enough system both random partitions and percolation γ_2 peaks at nearly the same value of
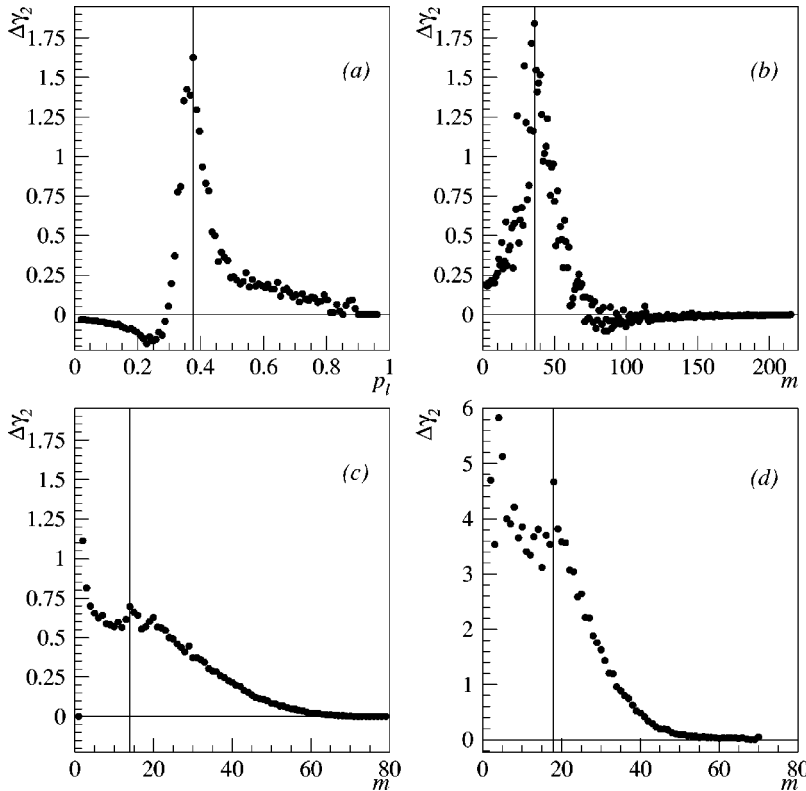

FIG. 4. The quantity $\Delta \gamma_2$ for (a) percolation ($A_0 = 216$) as a function of p_l, (b) percolation as a function of m, (c) random partitions as a function of m, and (d) Au + C multifragmentation as a function of m. Solid vertical lines indicate the guess for the critical point.
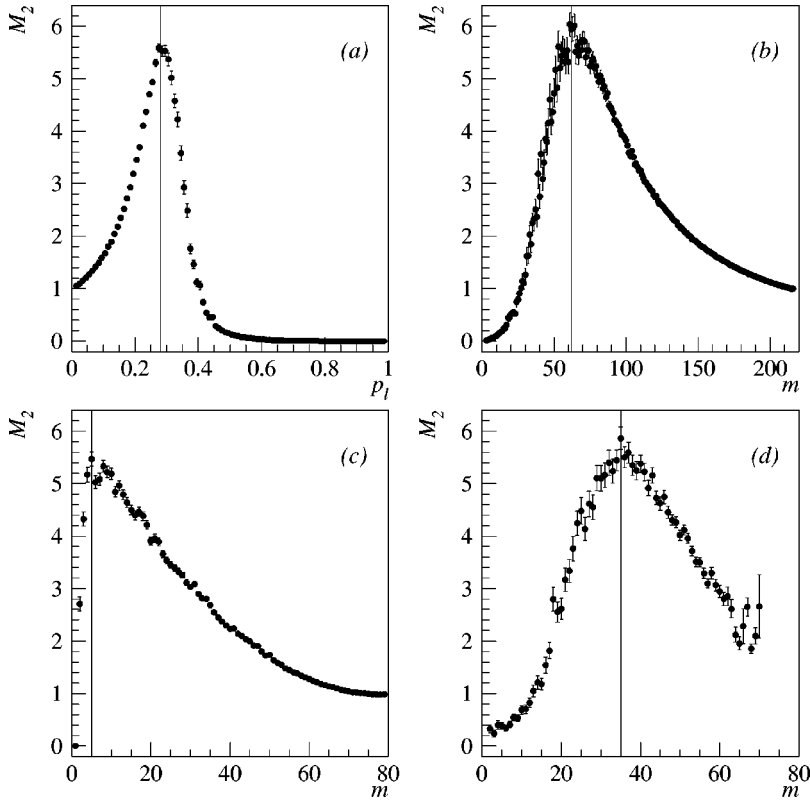
FIG. 5. The second moment M_2 of the cluster distributions for (a) percolation as a function of p_l, (b) percolation as a function of m, (c) random partitions as a function of m, and (d) Au + C multifragmentation as a function of m. Solid vertical lines indicate the guess for the critical point.

the control parameter regardless of the method of averaging used. For the percolation system the value of p_l at the peak in γ_2 is close to the value of p_l where $\Delta(A_{\max}/A_0)$ is a maximum. This coincidence does not hold for random partitions; compare Figs. 1(c) and 4(c). For both percolation (m) and multifragmentation, there is better agreement on the critical point from fluctuations and than from γ_2 was computed via Eq. (24).

2. Divergences

Another signature used previously to infer the existence of a continuous phase transition from cluster distributions is the observance of a peak in the second moment [15,70]. However, it has been pointed out that models with no phase transition can exhibit a peaking behavior in the second moment [55]. Figure 5 shows the behavior of the second moment for each of the systems examined in this work. In this figure, for the sake of illustration, the largest cluster has been excluded from the sum at all values of the control parameter. Each system shows a peak at some intermediate value of its control parameter. Table I lists the location of the second moment peaks. It is clear from the peak observed for the random partitions that it is possible to observe a peak in the second moment for a noncritical cluster distribution. Thus this behavior alone cannot be used to distinguish between critical and noncritical systems.

An issue with the use of the second moment's peaking behavior is the exclusion of the largest cluster from the sum in Eq. (14). Again, in the FDM formalism the sum runs over all clusters in the *gas*. On the *liquid* side of the critical point a gas exists in addition to a liquid drop. Thus, the largest

cluster represents the bulk liquid. On the *gas* side of the critical point there is no liquid drop and the largest cluster is merely the largest gas particle. With this understanding it is clear that the largest cluster should be omitted from the summation in the second moment only in the *liquid* region, whereas the summation should run over all clusters in the *gas* region. For a proper construction of the second moment, knowledge of the location of the critical point is required. In the thermodynamic limit of infinite system size, exclusion of the largest cluster makes little difference. However in small systems the proper construction of the second moment is crucial if critical behavior is to be observed in Ref. [71].

3. Campi plots

Plots of the natural log of the normalized size of the largest cluster $\ln(A_{\max}/A_0)$ versus the natural log of the second moment $\ln(M_2)$ were first presented by Campi in a comparison of gold multifragmentation and percolation [15]. Figure 6 shows the resulting plots for each of the systems discussed in this paper. In each plot there is a liquid leg for the largest $A_{\max}$ and small M_2 and a gas leg for smaller $A_{\max}$ and midrange values of M_2. That similar behavior is observed for all systems is *an* indication that this is a necessary, but not sufficient observation for critical behavior. Quantitative information extracted from such plots may indeed be consistent with known ratios of critical exponents. This has been done recently for peripheral collisions between gold nuclei at $35A$ MeV [72].

4. Rise and fall of intermediate mass fragments

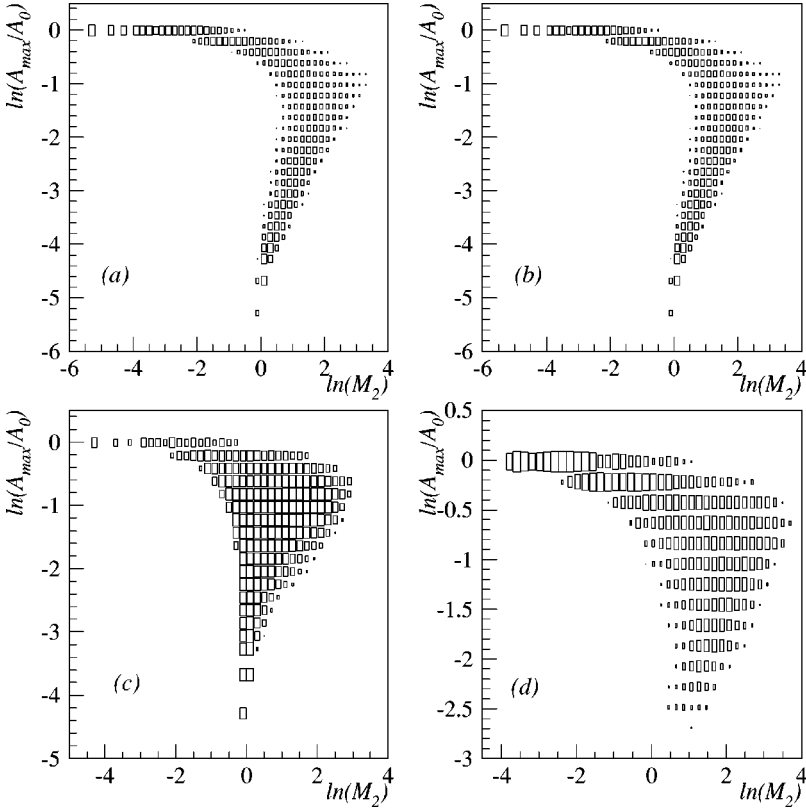In many nuclear multifragmentation studies the term ''intermediate mass fragment'' (IMF) has been defined as a clus-

FIG. 6. Campi plots of the cluster distributions for: (a) percolation as a function of p_l, (b) percolation as a function of m, (c) random partitions as a function of m, and (d) Au + C multifragmentation as a function of m.

ter which has a charge between $3 \leq Z_f \leq 30$. For the percolation system presented here a *charge* has been assigned to each cluster by multiplying the number of constituents in the cluster by the charge to mass ratio of a gold nucleus. For the random partitions the number of constituents is used as the *charge*. Since the definition of an IMF is arbitrary, the precise boundaries of the range in cluster size used makes little qualitative difference.

Aside from the equilibrium arguments made by the ALIDIN group [49–51], little insight towards the presence or absence of a continuous phase transition is gained from a plot of the average number of IMF's $\langle M_{\mathrm{IMF}} \rangle$ versus the control parameter. Figure 7 shows the results for the systems discussed in this work. Each system shows a peak in $\langle M_{\mathrm{IMF}} \rangle$ at some intermediate value of the control parameter. Comparing the peak position in Fig. 7 to the values listed in Table I shows that there is little correspondence between the various proposed methods for locating the critical point. The arbitrary nature of the definition of an IMF makes it unlikely that the peak in $\langle M_{\mathrm{IMF}} \rangle$ occurs precisely at the critical point. To some degree the rise and fall feature is due to the constraint of a fixed number of constituents. It it obvious that a the extreme values of the control parameter, the number of IMFs must diminish, while at intermediate values, it must be at least as great. Thus, the occurrence of a peak at some intermediate value of the control parameter is expected.

5. τ_{eff} *minimum*

With the first observation of a power law in the nuclear multifragmentation yield distribution [5,11] it became a common analysis tool to fit cluster distributions to a power

laws and extract exponent values. In an effort to make this a more quantitative analysis the value of the extracted exponent τ_{eff} was examined as a function of some control parameter that was experimentally or numerically accessible. It was assumed that at the critical point the value of τ_{eff} should attain a lower value than fits which were performed away from the critical point [73–78]. The logic of this assumption was based upon the idea that at low *temperatures* a system has few small clusters, so the power law should be steep, leading to a high τ_{eff} value. At high temperatures there are many small clusters and little else, which is reflected in a high value of τ_{eff} and a steep power law. At the critical point clusters on all length scales appear and the power law is shallow with a lower value of τ_{eff}. In this analysis the largest cluster was omitted from the fitting procedure and both the constant of proportionality and τ_{eff} were allowed to vary independently. Many investigations of nuclear multifragmentation, both theoretical and experimental, employed this method of analysis [73–78].

One flaw in this analysis method is the use of a two parameter fit for the power law. Allowing both the overall normalization of the power law and the exponent to vary independently is in conflict with the scaling assumptions underlying the FDM as shown in Eqs. (8) and (9). A proper fit for a power law within the context of the FDM should be based on single parameter; as such, the cluster distribution must be normalized to the size of the system as was outlined in Sec. III.

Leaving aside for a moment that the execution of the τ_{eff}-minimum analysis violates the scaling assumptions of the FDM, the signal of a minimum in the cluster yield power
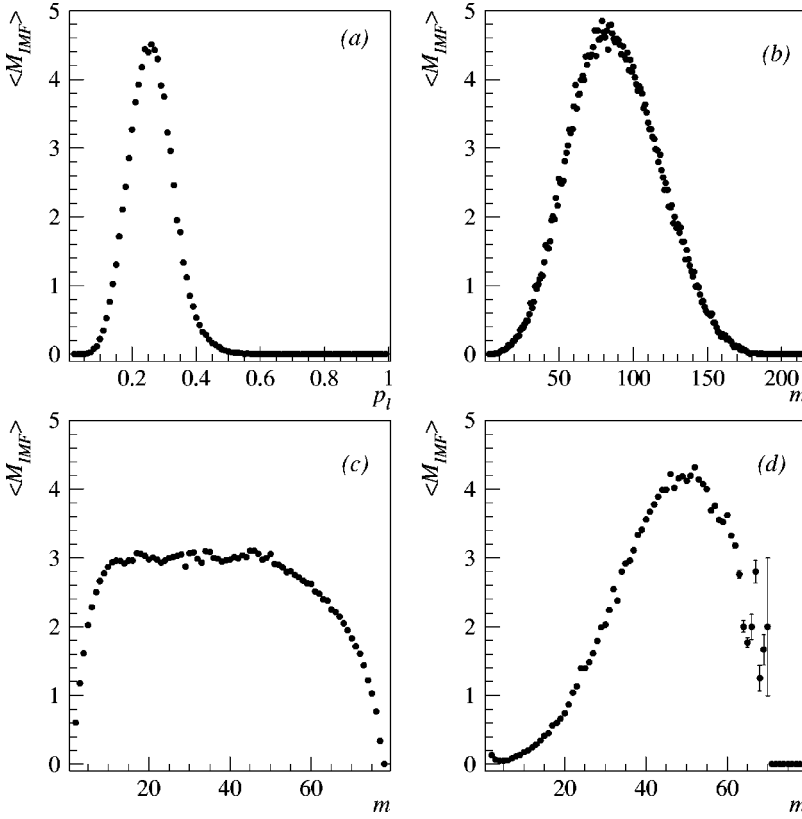
FIG. 7. Average number of intermediate mass clusters $\langle M_{\text{IMF}}\rangle$ for (a) percolation as a function of p_l, (b) percolation as a function of m, (c) random partitions as a function of m, and (d) Au + C multifragmentation as a function of m.

law will be examined. A two parameter fit for τ_{eff} searches for the minimum in an effective exponent which is defined as [79–81]:

$$\tau_{\text{eff}} = -\frac{\partial \ln n_{A_f}(\epsilon)}{\partial \ln A_f}. \tag{26}$$

Assuming that the system under study follows a power law in the cluster yield at the critical point, and away from the critical point the cluster yield is affected by a scaling function such as in Eq. (7), then

$$\tau_{\text{eff}} = \tau - A_f \frac{\partial \ln f}{\partial A_f}. \tag{27}$$

The minimum in τ_{eff} can be found by differentiating Eq. (27):

$$\frac{d\tau_{\text{eff}}}{d\epsilon} = -A_f \frac{\partial}{\partial \epsilon} \frac{\partial \ln f}{\partial A_f} = 0. \tag{28}$$

The location of the minimum in τ_{eff} is dependent on the form of the scaling function f. Assuming the scaling function has the form of Eq. (4) then the minimum in τ_{eff} will be at $\epsilon = B/2A_f^\sigma$, not at the critical point $\epsilon_c = 0$.

Despite the flaws in the τ_{eff}-minimum analysis it is of interest to examine the results for the systems discussed in this paper. Figures 8–11 show the results for a two parameter fit to the cluster distribution for percolation (probability and multiplicity), random partitions and gold multifragmentation,

respectively. For all systems, the cluster distributions were fit at each value of the control parameter. Only clusters with $\sim 0.02 \lesssim (A_f/A_0) \lesssim \sim 0.22$ were included in the fits. The first three systems weighted χ_ν^2 with errors associated with $n_{A_f}(\epsilon)$ while the χ_ν^2 for the gold multifragmentation cluster distributions were weighted with errors on both $n_{A_f}(\epsilon)$ and A_f.

For the percolation (p_l) a minimum in τ_{eff} was observed at $p_l = 0.3$ with $\chi_\nu^2 = 2.3$, $q_0 = 0.214 \pm 0.005$ and $\tau = 2.19 \pm 0.01$; shown in Figs. 8(a), 8(b), and 8(c) by the dotted lines. However, at $p_l = 0.33$ the $\chi_\nu^2 = 1.02$, $q_0 = 0.181 \pm 0.003$, and $\tau = 2.27 \pm 0.01$; shown in Figs. 8(a)–8(c) with the dashed lines. Based on a goodness of fit comparison, the latter value of p_l is a better choice for the critical point. This result is in agreement with the analytic discussion of τ_{eff} above, namely, that a minimum in τ_{eff} is a poor indicator of the critical point. If the results for $p_l = 0.33$ are compared to the center of the τ_{eff}, $p_l \sim 0.28$, the differences in the χ_ν^2 and q_0 results are even more striking.

Similar results were seen for percolation (m), see Fig. 9. Here the minimum in the τ_{eff} well yielded worse results for both χ_ν^2 and q_0 than does the choice of the critical point based on a choice from the $\chi_\nu^2 \sim 1$ region where there is good agreement between the fitted q_0 and the value computed using Eq. (9) and the canonical τ value for three-dimensional percolation.

Significant differences between percolation and random partitions are observed in this analysis as seen in Fig. 10. The solid lines show the τ_{eff} and q_0 values for systems in the three-dimensional Ising universality class, while the dashed line shows the τ_{eff} and q_0 for three-dimensional percolation.
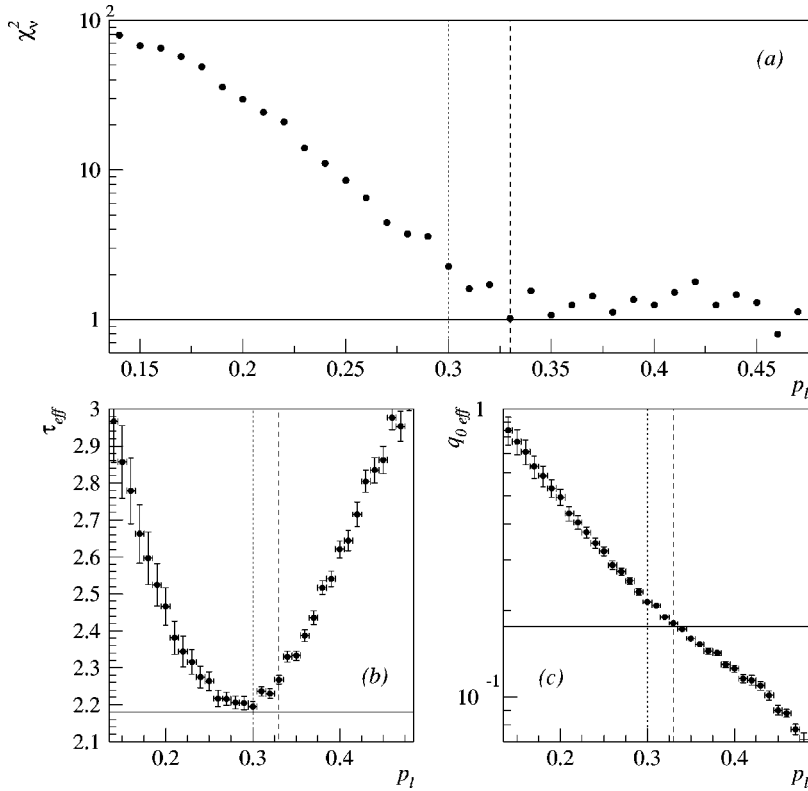
FIG. 8. Results for τ_{eff} minimum analysis on percolation as a function of p_l: (a) χ^2_ν, (b) fitted τ_{eff}, and (c) q_0. The vertical dotted lines show the location of the minimum in τ_{eff}. The vertical dashed line shows one instance of a better fit based on χ^2_ν. The horizontal solid lines show the accepted values of τ and q_0 for percolation.

The first noticeable difference is a lack of a valley shape in the plot of τ_{eff} versus control parameter, see Fig. 10(b). The value of τ_{eff} is below 2.2 for all but $m > 60$. Next is the lack of a region in m where $\chi^2_\nu \sim 1$ (other than at $m = 2$), see Fig. 10(a). All fits yield large χ^2_ν values indicating poor fits to the cluster distribution by a power law for the range of clusters examined.

The gold multifragmentation data show results similar to those of percolation (m). Here the cluster size is measured in terms of the nucleon number and the cluster distribution is normalized to the mass of the gold projectile remnant. Figure 11(b) shows a valley in τ_{eff} as a function of m, albeit one with a shallow and questionable upwards slope at high m. Figure 11(c) shows fitted values of q_0 that coincide with
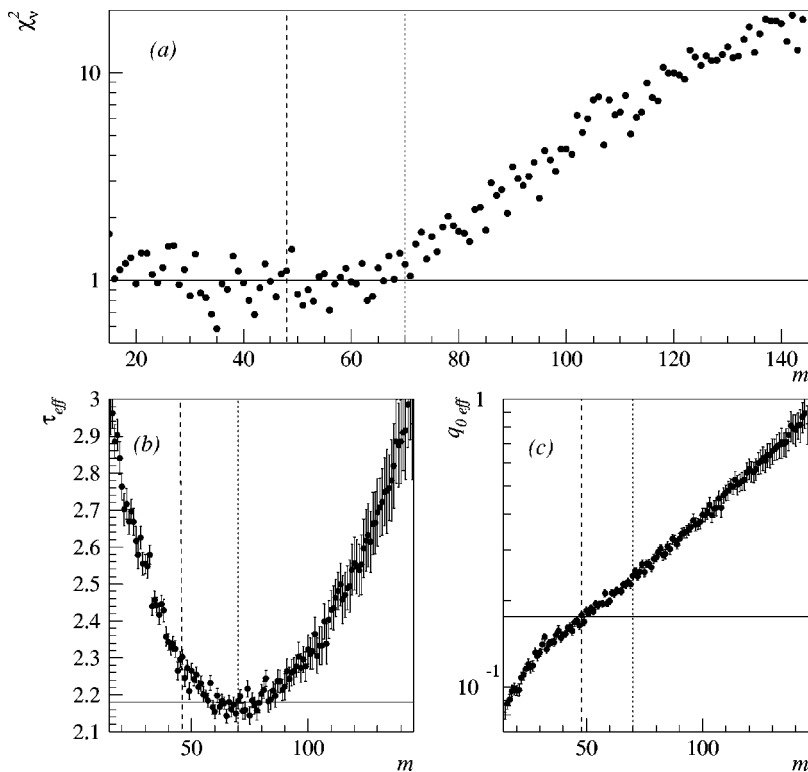

FIG. 9. Results for τ_{eff}-minimum analysis on percolation as a function of m: (a) χ^2_ν, (b) fitted τ_{eff} and (c) q_0. The vertical dotted line show the location of the minimum in τ_{eff}. The vertical dashed line shows one instance of of a better fit based on χ^2_ν. The horizontal solid lines show the accepted values of τ and q_0 for percolation.
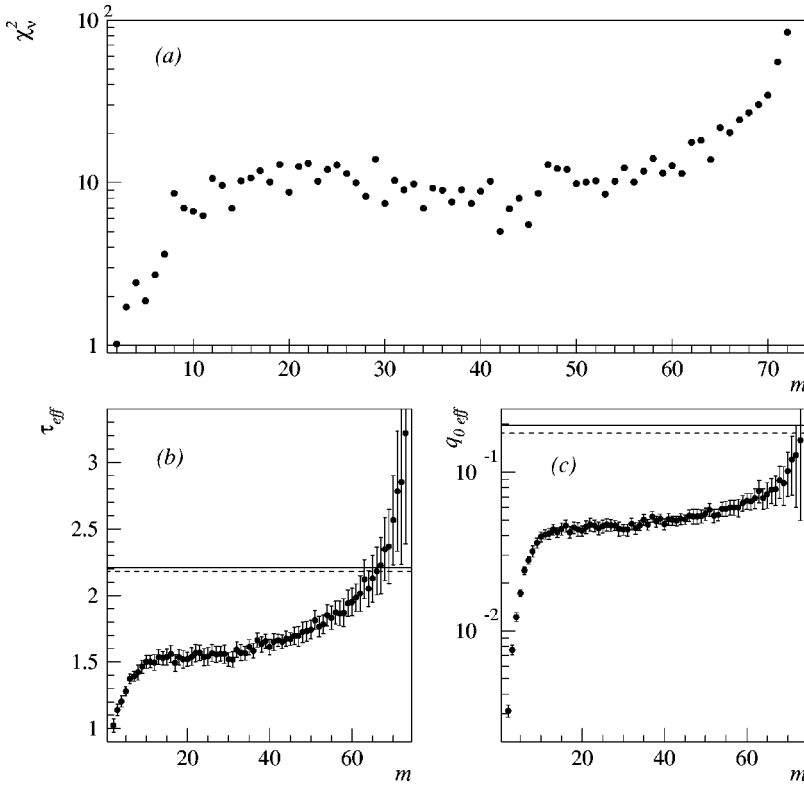
FIG. 10. Results for τ_{eff}-minimum analysis on random partitions: (a) χ_ν^2, (b) fitted τ_{eff}, and (c) q_0. The horizontal solid (dashed) lines show the accepted values of τ and q_0 for percolation (3D Ising).

canonical values. Figure 11(a) shows a region of low χ_ν^2 values followed by steadily increasing values. If no knowledge of the q_0 and τ values is assumed, then this analysis shows no definitive signals. The τ_{eff} valley shows a broad minimum in χ_ν^2 thus no one value of m can be selected for the critical point based on goodness of fit arguments. At best

one could argue for the neighborhood of the critical point and a value of q_0 and τ in some broad range.

6. Conclusion

The analyses presented above yield inconclusive results. All of the considered systems show similar signals which are
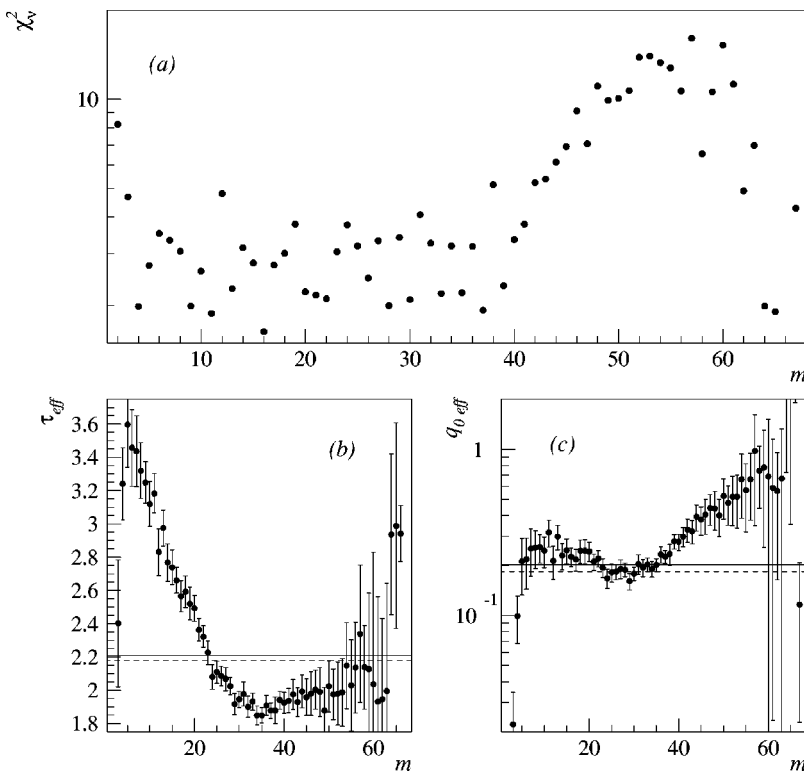

FIG. 11. Results for τ_{eff}-minimum analysis on Au + C multifragmentation: (a) χ_ν^2, (b) fitted τ_{eff}, and (c) q_0. The horizontal solid (dashed) lines show the accepted values of τ and q_0 for percolation (3D Ising).
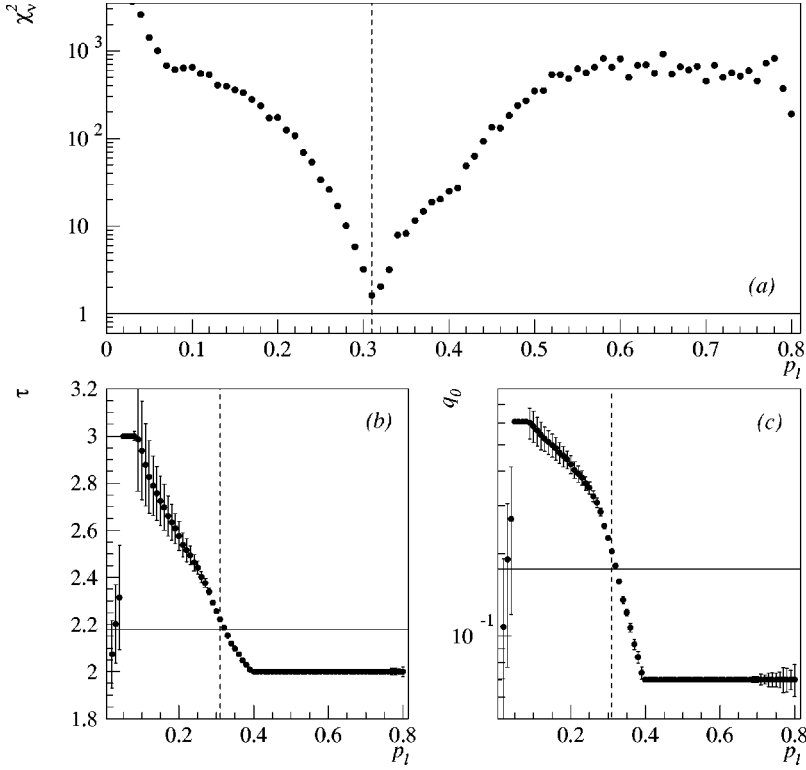
FIG. 12. Results for the full Fisher τ-power law analysis on percolation as a function of p_l: (a) χ^2_ν, (b) fitted τ, and (c) q_0. The vertical dashed line shows the estimate of the critical point based on a best fit based on χ^2_ν. The horizontal solid lines show the accepted values of τ and q_0 for percolation.

qualitative in nature and open to interpretation. It is therefore impossible, based solely on this level of analysis, to make a definitive conclusion as to the presence of a continuous phase transition in any of these systems. What is needed is an analysis or set of analyses that more clearly differentiates between systems with and without critical behavior.

B. Sensitive signatures

1. The Fisher τ-power law and the critical point

In this section the cluster yields are fit to a power law in a manner consistent with the FDM formalism. As with the two parameter fits the yields for clusters with $\sim 0.02 \lesssim (A_f/A_0) \lesssim \sim 0.22$ were fit at each value of the control parameter. However, only a single parameter, the value of τ, was allowed to vary to minimize the χ^2_ν of the fit. The value of the normalization q_0 was determined via the Riemann ζ function in Eq. (9). As suggested by Fisher [7], the value of τ was constrained to be between 2 and 3 so that the sum in the ζ function converges.

If the cluster distribution is well described by the FDM, then at the critical point the fit to a single parameter power law should show a minimum in χ^2_ν. Away from the critical point the power law is modified by a scaling function with a form similar to that given in Eq. (4). Therefore, fits to a single parameter power law should become worse as the modification from the scaling function increases away from the critical point.

Figure 12 shows the results for the percolation system with p_l as the control parameter. In Fig. 12(a), a minimum in χ^2_ν is observed for fits in the mid p_l range. This minimum indicates the location in p_l of the cluster yield distribution

which is best fit by a single parameter power law as suggested by the FDM formalism. By this estimation the critical point for this 216 site percolation lattice is at $p_c = 0.31 \pm 0.05$ with $\tau = 2.2 \pm 0.1$, $q_0 = 0.20 \pm 0.01$, and a $\chi^2_\nu = 1.62$. The precise canonical values of τ and q_0 are not extracted due in part to unavoidable finite size effects, and in part to the binning of cluster yields together over a range of 0.01 in p_l, which causes the *true* cluster distribution at the critical point to be contaminated by distributions at other values of the control parameter. In spite of these difficulties, the signature of the critical behavior suggested by the FDM formalism is evident. The location of the critical point determined here is consistent, at the 10% level, with the insensitive signatures presented in the previous section, see Table I. Figure 16(a) shows the best fit power law. For the percolation system clusters consisting of a single site are excluded from the fitting procedure. It is accepted that those clusters reflect the effects of the finite size of the system to a higher degree than larger clusters. Clusters with $A_f \lesssim 53$ were included in the fit. The largest cluster from each *event* was excluded from consideration when generating the average cluster distribution in keeping with the FDM formalism. Figure 16(a) shows the data for the entire cluster distribution in open circles. It is clear from this figure that the majority of the cluster distribution was used in the power law fit and further, that the exclusion or inclusion of the larger clusters has almost no effect on the results of this procedure. The extracted parameters, namely, τ, q_0, and p_c, do not depend on the fit range.

Figure 13 shows the results of the single parameter fit analysis when applied to the same percolation system but with the cluster multiplicity used as a measure of the con-
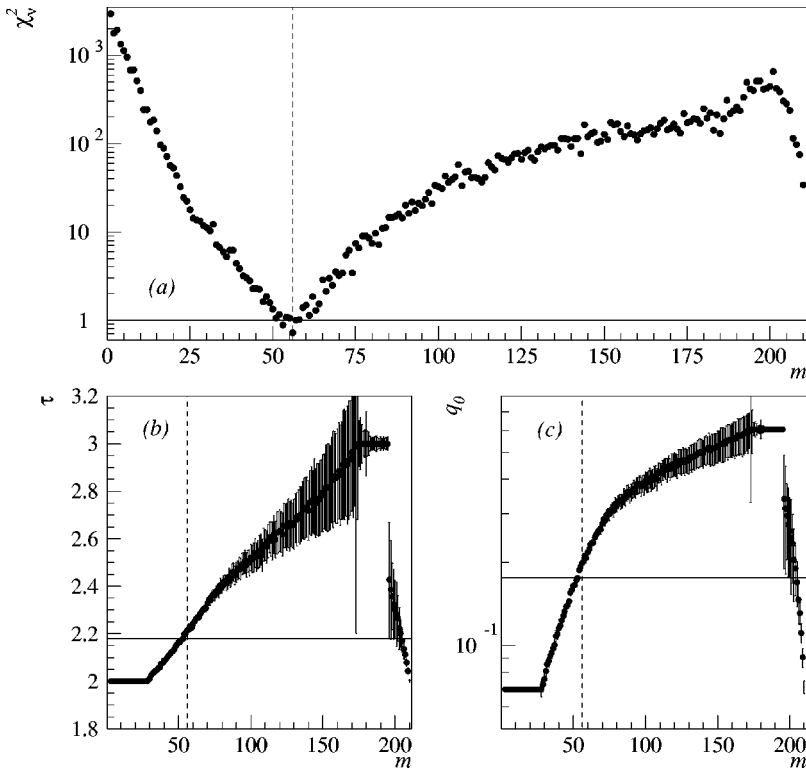
FIG. 13. Results for the full Fisher τ-power law analysis on percolation as a function of m: (a) χ_ν^2, (b) fitted τ, and (c) q_0. The vertical dashed line shows the estimate of the critical point based on a best fit based on χ_ν^2. The horizontal solid lines show the accepted values of τ and q_0 for percolation.

trolparameter. Again there is a minimum in the χ_ν^2 values at some intermediate value of the control parameter which indicates that $m_c = 57 \pm 3$ with $\tau = 2.2 \pm 0.1$, $q_0 = 0.20 \pm 0.01$, and $\chi_\nu^2 = 0.72$. Note the consistency between these values of q_0 and τ and those obtained with p_l following this method. The location of the critical point determined here is consistent, at the 10% level, with the insensitive signatures presented in the previous section. The lower χ_ν^2 value is due to the finer bins over which the cluster distributions were grouped. Figure 16(b) shows the best fit power law. Here only clusters of size $A = 1$ and size $A = A_{max}$ were excluded from the fitting procedure.

From Figs. 12 and 13 it could be argued, based on the best agreement between the fitted τ and the accepted three dimensional percolation value, that there are better choices for the critical point than those quoted above. However, those arguments assume knowledge of the value of τ as an input. The use of the location of the best fit to a single parameter power law as an indicator of the critical point makes no assumption regarding the value of τ and is a test of the FDM formalism in which only the range of τ is suggested: $2 < \tau < 3$. The values of τ and q_0 are outputs rather than inputs of this analysis. Much of the following analysis presented in this paper follows the same philosophy. That is, the analysis is designed to test the cluster distribution in question for behavior consistent with the FDM formalism. The values of quantities, such as critical exponents, are results of the analysis method and are in no way selected for on the basis of their particular values. Agreement between exponent values determined by this procedure and the canonical values in various universality classes is then significant because the values of the exponents are determined solely by the behavior of the cluster distributions so analyzed.

The results of the single parameter power law fits for the random partitions are presented in Fig. 14. There is a minimum in the χ_ν^2 value at $m = 59$. However $\chi_\nu^2 = 10.83$, which is an order of magnitude above the percolation results, should not be used as an indication of a good fit of the cluster distribution by a single parameter power law. The location of the χ_ν^2 minimum is also in disagreement with the insensitive signatures presented in the last section. Here only clusters of size $A_f = 1$ and size $A_f = A_{max}$ were excluded from the fitting procedure.

Figure 15 shows the results of this analysis applied to the gold multifragmentation data. As with the percolation results, the χ_ν^2 shows a minimum that drops nearly two orders of magnitude from the peaks for high and low m to the valley at a midrange value of m, see Fig. 15(a). In the context of the FDM analysis this result suggests that the critical point is located at $m_c = 22 \pm 1$ with $\tau = 2.2 \pm 0.1$ and $q_0 = 0.18 \pm 0.01$ and $\chi_\nu^2 = 2.70$. The best fit power law is show in Fig. 16(d). An uncertainty of one unit of multiplicity is assigned to m_c to take into account the relatively low values of χ_ν^2 of the neighboring fits.

For the above fits to the gold multifragmentation data the χ_ν^2 is weighted by the errors in both n_{A_f} and A_f. The fitting procedure has also been performed with no error weighting on χ_ν^2 and with errors only in n_{A_f} for weighting. Both analyses shows results that were not significantly different from those quoted here. As mentioned previously, clusters with $Z_f = 2$ are created in both the prompt first stage and in the multifragmenting of the gold nuclear remnant. The prompt $Z_f = 2$ clusters have been excluded from the gold multifragmentation analysis. As a further test of the single parameter power law fit, only clusters with $3 \leq Z_f \leq 16$, i.e., clusters
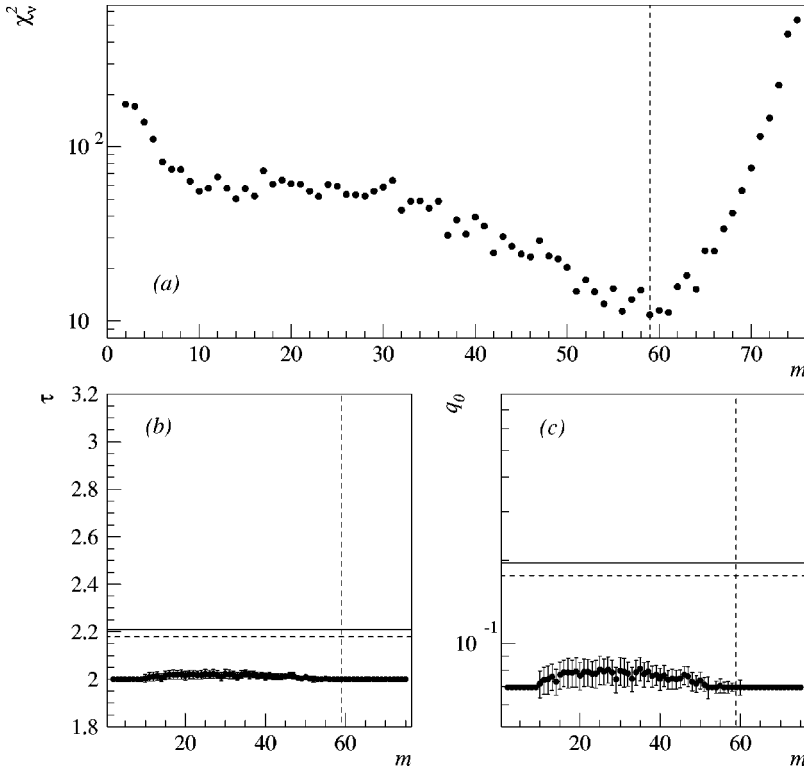
FIG. 14. Results for the full Fisher τ-power law analysis on random partitions: (a) χ_ν^2, (b) fitted τ, and (c) q_0. The horizontal solid (dashed) lines show the accepted values of τ and q_0 for percolation (3D Ising).

with no contamination from the prompt first stage, were included in a repeat of this analysis. Again the results show practically the same behavior as those shown here. As yet another test, clusters with $2 \leqslant Z_f < Z_{max}$ were included in the fitting procedure, and again the results showed little difference from those presented here. Finally clusters with $3 \leqslant Z_f < Z_{max}$ were included in the fitting procedure, and again the

results showed no difference from those presented here. The data consistently exhibited a deep valley in the χ_ν^2 versus m plot which indicated that the location of the critical point was $m_c \sim 22$ and that $\tau \sim 2.2$, $q_0 \sim 0.18$ and $1 < \chi_\nu^2 < 4$. Thus the value of τ and the location of m_c are not sensitive to the fit region. The behavior of the data show this clearly, see open circles in Fig. 16(d).
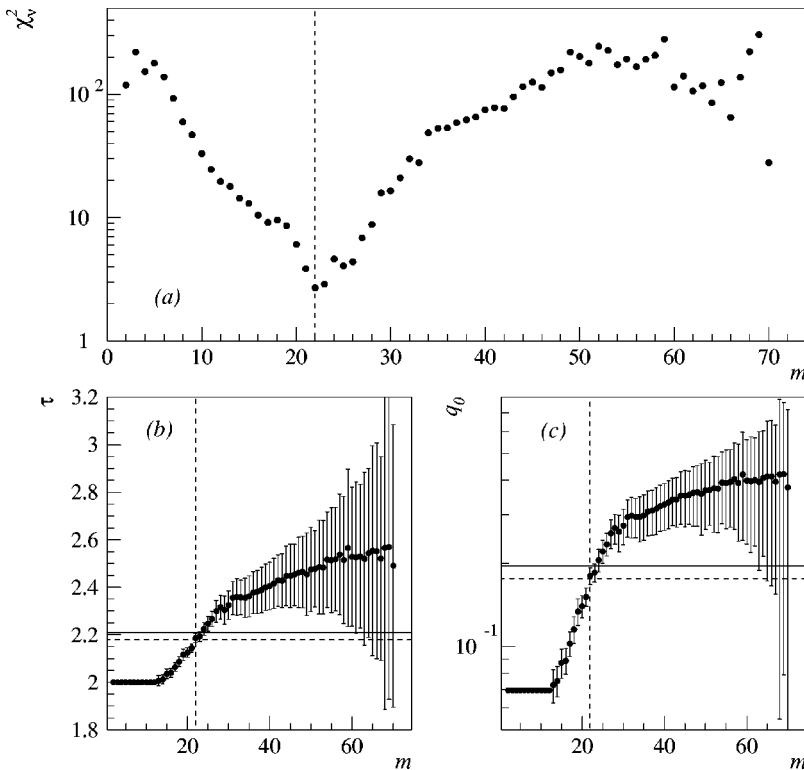

FIG. 15. Results for the full Fisher τ-power law analysis on Au + C multifragmentation: (a) χ_ν^2, (b) fitted τ, and (c) q_0. The vertical dashed line shows the estimate of the critical point based on a best fit based on χ_ν^2. The horizontal solid (dashed) lines show the accepted values of τ and q_0 for percolation (3D Ising).
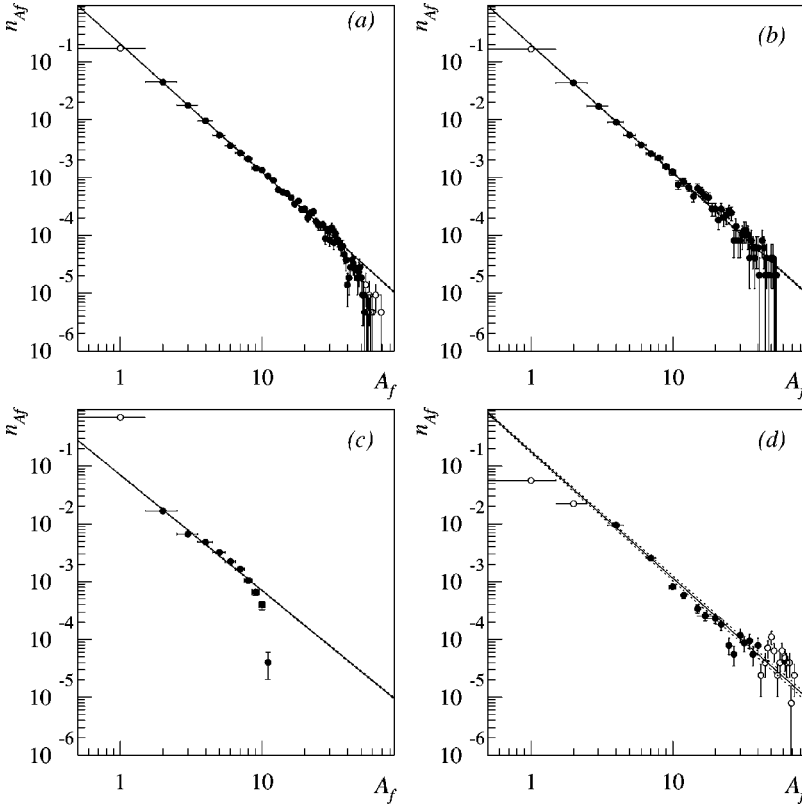
FIG. 16. Best fit Fisher τ-power laws for (a) percolation (p_l), (b) percolation (m), (c) random partitions, and (d) Au + C multifragmentation. Solid circles were included in the fits, open circles were excluded. Solid lines show the best fit power law, dotted lines indicate error in the power law based on errors in the fitted parameters.

The single parameter power law analysis of the cluster distributions of the various systems yielded a result which differentiated between systems that follow the FDM formalism and systems that do not. The differences between Figs. 12(a), 13(a), 15(a), and 14(a) are clear. For both percolation and gold multifragmentation the behavior of χ_ν^2 was just as predicted by the FDM formalism for continuous phase transitions. Far from the critical point the cluster distribution was fit poorly by a single parameter power law due to the influence of a scaling function where volume and surface effects overwhelm the underlying power law. At the critical point, where the influence of the scaling function vanishes, the cluster distributions were well described by a single parameter power law with an exponent value $\tau \sim 2.2$ and thus $q_0 \sim 0.2$, in keeping with what is expected for many universality classes. This fitting procedure does not merely search out a cluster distribution which is well fit by a power law, but finds the cluster distribution which is well fit by the FDM formalism. This is achieved via the coupling between the exponent τ and the normalization factor q_0, see Eq. (9). The random partitions fail to produce such signals. This is expected as that system does not obey the FDM formalism and thus should not show the same signals as systems that are known to follow the FDM such as percolation. This analysis of the cluster yield of gold multifragmentation yields a signal that is suggestive of critical phenomenon in keeping with the FDM formalism.

2. The critical exponent σ

In Sec. III it was shown that in the context of the FDM the surface of a cluster makes a contribution to the free energy of

cluster formation, via the scaling function $f(z)$, that depends on the number of constituents of the cluster raised to the power σ; see Eqs. (1), (4), and (5). Therefore, it is possible to determine the value of σ by examining cluster production as a function of the control parameter. To see this, consider that the behavior of the order parameter suggests that the scaling function $f(z)$ has a maximum [61]. At the maximum of the scaling function $f_{\max}(z_{\max})$, the production of A_f sized clusters is greatest:

$$n_{A_f}^{\max}(\epsilon_{\max}) = q_0 A_f^{-\tau} f(z_{\max}). \qquad (29)$$

The argument of $f_{\max}$ is

$$z_{\max} = A_f^{\sigma} \epsilon_{\max}, \qquad (30)$$

where the value of $z_{\max}$ depends on the specific details of the system in question [63]. Rearranging Eq. (30) yields

$$\epsilon_{\max} = z_{\max} A_f^{-\sigma}. \qquad (31)$$

Thus $\epsilon_{\max}$, the value of the control parameter at which the greatest number of clusters of size A_f are produced, is related to the cluster size through a simple power law with exponent σ. The exponent σ can then be determined from knowledge of the location of the critical point and the value of the control parameter at the greatest production of clusters of size A_f.

The location of the critical point was determined in the search for the Fisher τ-power law in Sec. IV B 1 and will be used here to determine the σ. The value of the control parameter which yields the greatest production of each A_f clus-
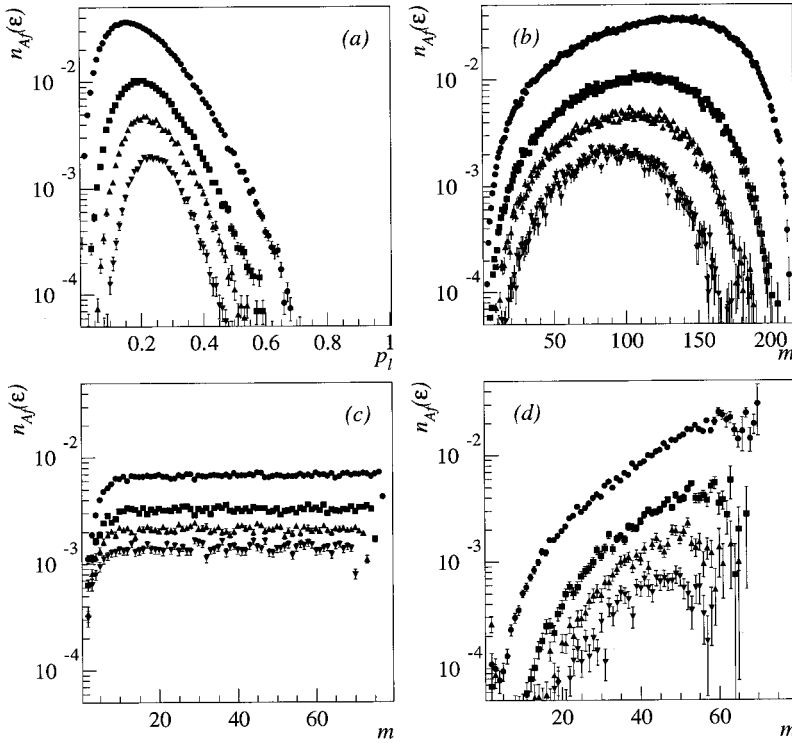
FIG. 17. Rise and fall in the production of individual clusters for (a) percolation as a function of p_l, (b) percolation as a function of m, (c) random partitions as a function of m, and (d) Au + C multifragmentation as a function of m. Symbols ($\bullet$, $\blacksquare$, $\blacktriangle$, $\blacktriangledown$) indicate clusters of size (charge) 3, 5, 7, and 10 for percolation and random partitions (multifragmentation).

ter size was determined from the peak location in a plot of $n_{A_f}(\epsilon)$ versus the system's control parameter, see Fig. 17.

For each system at each cluster size plots such as those shown in Fig. 17 were used to determine the location of the peak of $n_{A_f}(\epsilon)$. For example, in percolation (p_l), $\epsilon_{\max} = (p_c - p_{\max})/p_c$, pairs of points $[n_{A_f}(\epsilon), p_l]$ for a particular A_f were fed into a SPLINE routine [82]. Input pairs were then *smeared* by assigning $\delta n_{A_f}(\epsilon)$ as the standard deviation of a Gaussian centered on $n_{A_f}(\epsilon)$. Output of the SPLINE routine was used to interpolate the behavior of a smooth curve between the pairs of input points. Stepping along the interpolations in increments much smaller than the separation of the input p_l, a maximum of $n_{A_f}(\epsilon)$ was determined and $p_{\max}$ was recorded. This process was repeated thousands of times for each cluster size and lead to an estimate of $p_{\max} \pm \delta p_{\max}$ as a function of A_f.

Using $p_{\max}(A_f) \pm \delta p_{\max}(A_f)$ and the value of $p_c \pm \delta p_c$, from the Fisher τ-power law determination process, the value of the exponent σ was determined by taking the slope of $\ln(\epsilon_{\max})$ versus $\ln(A_f)$. The value of $z_{\max}$ was determined by exponentiating the offset. The value of p_c was varied uniformly throughout the range suggested by δp_c and tens of fits were made with varying starting and ending points in A_f of the fitting region. The final value of $\sigma \pm \delta\sigma$ and $z_{\max} \pm \delta z_{\max}$ are the average and RMS values resulting from all the fits.

Results of this analysis performed on percolation (p_l) are shown in Fig. 18(a). Here the value of the control parameter that coincides with the maximum in production of clusters of size A_f, $\epsilon_{\max}$, is plotted against the cluster size. Results of the average power law fits to Eq. (31) are plotted as a solid line. The agreement between the values returned by the pro-

cedure discussed above, $\sigma = 0.52 \pm 0.02$ and $z_{\max} = -0.89 \pm 0.03$, and the accepted values for three-dimensional percolation, $\sigma = 0.45$ and $z_{\max} = -0.8$ [63], establishes the reliability of this exponent extraction method. The analysis differs in method from previous efforts on percolation lattices [71,83] but not in result.

The next test of this analysis is to extract a value of σ from percolation (m). In order for this procedure to be useful on multifragmentation data it must be demonstrated that the exponent σ can be determined using cluster multiplicity as the control parameter. To that end the multiplicity at which the production of each cluster size is maximal, $m_{\max}$ was determined via the procedure described previously. Using the value of $m_c \pm \delta m_c$ determined via searching for the Fisher τ-power law and $m_{\max}$ the exponent σ was determined by taking the slope of $\ln(\epsilon_{\max})$ versus $\ln(A_f)$. The value of m_c was varied uniformly throughout the range suggested by δm_c and several fits were made with varying starting and ending points in A_f of the fitting region. The value of $z_{\max}$ was determined by exponentiating the offset. Results of the average power law fits to Eq. (31) are plotted as a solid line in Fig. 18(b). The agreement between the values returned by this procedure, $\sigma = 0.52 \pm 0.02$, the value for σ quoted above, and the accepted values for three-dimensional percolation again establishes the reliability of this exponent extraction method and shows that the use of m as a control parameter is acceptable.

The value of $z_{\max} = -2.4 \pm 0.1$ extracted for percolation as a function of multiplicity is different from the value quoted above, $z_{\max} = -0.89 \pm 0.03$, for the percolation system as a function of probability. This is a result of changing the measure of the control parameter from probability to multiplicity. This difference was observed in previous percolation efforts
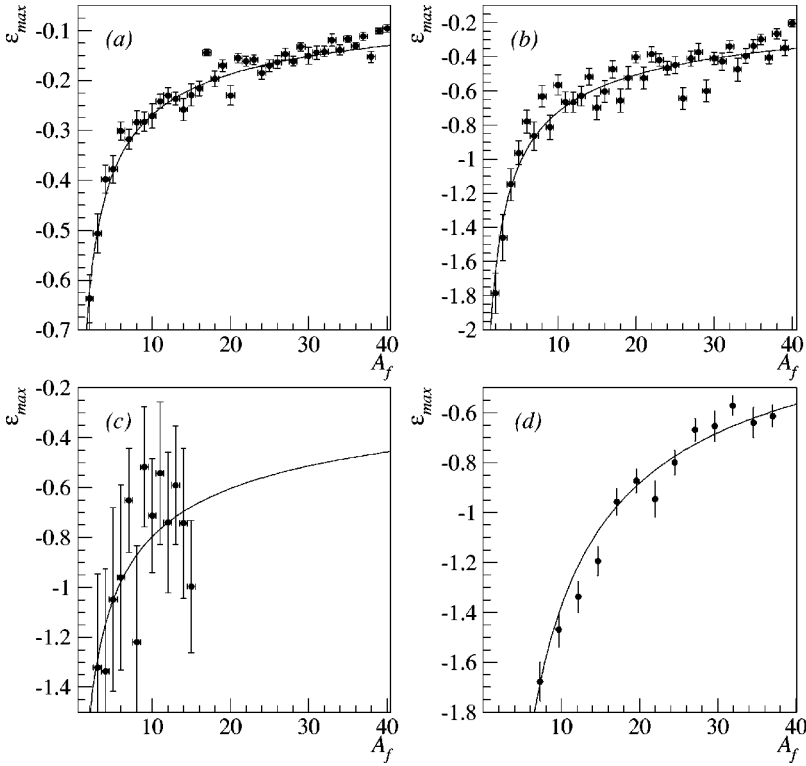
FIG. 18. Results of the σ extraction procedure for (a) percolation as a function of p_l, (b) percolation as a function of m, (c) random partitions as a function of m, and (d) Au + C multifragmentation as a function of m.

[83] and explained therein. A plot of $\epsilon(p_l)$ against $\epsilon(m)$ show that $z_{\max}(p_l)$ and $z_{\max}(m)$ map to each other. See Fig. 9 of Ref. [83].

Clusters from the random distribution were also subjected to this analysis. Due to the failure of the search for the Fisher τ-power law in the random partitions, the value of m_c determined in the analysis of the gold multifragmentation was used, $m_c = 22 \pm 1$. The value of the cluster multiplicity for maximum production of A_f sized clusters was determined in the same manner as with the percolation system. The flatness of the $n_{A_f}(\epsilon)$ versus m curves, see Fig. 17(c), makes finding a unique value of $m_{\max}$ impossible. This is reflected in the large error bars on $\epsilon_{\max} \pm \delta\epsilon_{\max}$ seen when plotted against A_f in Fig. 18(c). The value of $m_{\max}$ reported by the peak finding procedure employed here reflects, approximately, the midpoint of the multiplicity range of $n_{A_f}(\epsilon)$ for a particular A_f. Coupling the m_c from the filtered gold multifragmentation data with the $m_{\max}$ and fitting $\ln(\epsilon_{\max})$ versus $\ln(A_f)$ gave $\sigma = 0.4 \pm 0.2$ and $z_{\max} = -2.0 \pm 0.8$. However, it is clear when comparing the resulting average fit for the random partitions shown in Fig. 18(c) with either of the percolation results shown in Fig. 18(a) that the σ resulting for the random partitions cluster distribution is meaningless. This is to be expected as the framework of the FDM, used in the extraction of the exponent σ, is meaningful only when applied to systems which undergo a continuous phase transition. The *failure* of this analysis on this system is expected based on the basis of the *failure* of the analysis in the preceding section that aimed to find the Fisher τ-power law and the critical point.

Results for the extraction of σ from the gold multifragmentation data have been published previously [13,14]. In those analyses the largest cluster was excluded from consideration at every value of the control parameter. This is at odds with the formalism of the FDM where the sums excludes the largest cluster for $\epsilon > 0$ and include the largest cluster for $\epsilon < 0$.

The previous analyses yielded values of $\sigma = 0.68 \pm 0.05$ and 0.65 ± 0.06 for work with the un-normalized charge distribution and normalized mass distribution respectively. When this analysis was redone using formalism of the FDM, i.e., the largest cluster excluded on one side of the critical point (liquid) and included on the other side (gas), the values of σ were reduced by approximately 50%: $\sigma = 0.32 \pm 0.02$. In the case of percolation the difference introduced in the value of σ when following the FDM formalism (as was done above) or not (as was the case in Ref. [83]) is on the order of a few percent.

One source of this differing behavior between multifragmentation and percolation is the changing mass of the system. For gold multifragmentation, from $A_0 \sim 194$ at low m to $A_0 \sim 92$ at high m [60], while the system size is constant for percolation. For gold multifragmentation effects of the finite size of the system are felt more at high multiplicities than low. Since the percolation system size is constant, finite size effects are felt more evenly.

It is the higher values of m where cluster production peaks in multifragmentation. The finite size of the system limits the size to which a cluster can grow. Thus the number of clusters of size A_f, n_{A_f}, as a function of m is *contaminated* when the largest cluster $A_{\max}$ is included in a plot of n_{A_f} versus A_f because $A_{\max}$ *would like* to be larger, but finite size effects limit the size $A_{\max}$ can attain. Therefore, one method to account for this effect is to exclude $A_{\max}$ from the cluster dis-

TABLE II. Critical exponents.

Exponent/system	3D percolation	Percolation (p_l)	Percolation (m)	Random partitions	Au + C	3D Ising
τ	2.18	2.2 ± 0.1	2.2 ± 0.1	2.0 ± 0.1	2.2 ± 0.1	2.21
σ	0.45	0.52 ± 0.02	0.52 ± 0.02	0.4 ± 0.2	0.64 ± 0.05	0.64
$\gamma=\dfrac{3-\tau}{\sigma}$	1.82	1.5 ± 0.2	1.5 ± 0.2	2.5 ± 1.2	1.3 ± 0.2	1.23
γ_+ (matching)		1.8 ± 0.2	1.64 ± 0.04	0.4 ± 0.1	1.4 ± 0.3	
γ_- (matching)		1.8 ± 0.2	1.7 ± 0.1	0.5 ± 0.2	1.4 ± 0.3	
$\langle\gamma\rangle$ (matching)		1.8 ± 0.2	1.67 ± 0.05	0.5 ± 0.1	1.4 ± 0.3	
$\Delta\gamma$ (matching)		0.0 ± 0.3	0.06 ± 0.1	0.1 ± 0.2	0.0 ± 0.4	
ν (hyperscaling)	0.87	0.77 ± 0.07	0.77 ± 0.07		0.63 ± 0.07	0.63

tribution at large m values where these effects are largest. This was done for the gold multifragmentation data.

The multiplicity at which the production of each cluster size is maximal, m_{max} was determined via the procedure described previously. The value of m_c determined in the Fisher τ-power law analysis was used, $m_c=22\pm1$. The value of m_c was varied uniformly throughout the range suggested by δm_c and several fits were made with varying starting and ending points in A_f of the fitting region. The exponent σ was determined by taking the slope of $\ln(\epsilon_{max})$ versus $\ln(A_f)$ and the value of z_{max} was determined by exponentiating the offset. The results were $\sigma=0.64\pm0.05$ and $z_{max}=-6.0\pm0.8$, see Tables II and III. The average power law fits are shown in Fig. 18(d).

3. The scaling function $f(z)$

With the critical point (p_c or m_c), τ, q_0, and σ determined and assuming coexistence, $g=1$, it is possible to find the scaling function by rewriting Eq. (6) as

$$n_{A_f}(\epsilon)/q_0 A_f^{-\tau}=f(z). \qquad (32)$$

Doing this has the effect of appropriately scaling $n_{A_f}(\epsilon)$ and collapsing the data onto a single curve. Figure 19 shows the results of this sort of scaling.

In Figs. 19(a), 19(b), and 19(d), the data from percolation (p_l and m) and multifragmentation, respectively, show collapse onto a single curve for a wide range in cluster size and over nearly the full range in control parameter. Random partitions shows no such collapse, see Fig. 19(c).

As a demonstration of this type of collapse the same data has been scaled in the same fashion, but with a different choice of the critical point. Figure 20 shows the systems using a critical point with a value of half of the critical point determined via the Fisher τ-power law, while Fig. 21 shows the same analysis with a value of twice the critical point determined via the Fisher τ-power law. A visual inspection of Figs. 19, 20, and 21 reveals the greatest data collapse occurs when the choice of the Fisher τ-power law critical point is used, at least for the percolation (p_l and m) and multifragmentation systems. Random partitions show no such collapse. Using different values of τ and σ in this scaling analysis of random partitions does not significantly alter

TABLE III. Critical amplitudes.

| Amplitude/system	Percolation (p_l)	Percolation (m)	Random partitions	Au + C
q_0	0.20 ± 0.01	0.20 ± 0.01	0.07 ± 0.01	0.18 ± 0.01
z_{max}	-0.89 ± 0.03	-2.4 ± 0.1	-2.0 ± 0.8	-11.0 ± 2.0
z_{max} (scaling fcn)	-0.9 ± 0.1	-2.5 ± 0.5	-2.0 ± 8.0	-9.0 ± 2.0
Γ_+ (scaling)	0.9 ± 0.1	4.9 ± 0.5	3.5 ± 0.5	19.0 ± 3.0
Γ_- (scaling)	0.17 ± 0.05	0.3 ± 0.1	1.0 ± 0.2	0.24 ± 0.05
Γ_+/Γ_- (scaling)	5.0 ± 2.0	16.0 ± 6.0	3.5 ± 0.9	80.0 ± 20.0
Γ_+ (matching)	1.0 ± 0.3	7.0 ± 0.6	26.0 ± 2.0	26.0 ± 9.0
Γ_- (matching)	0.08 ± 0.07	0.28 ± 0.04	3.7 ± 0.4	0.27 ± 0.06
Γ_+/Γ_- (matching)	13.0 ± 12.0	25.0 ± 4.0	7.0 ± 1.0	100.0 ± 40.0
Γ_+ (C.T.S. 3dP)	0.9 ± 0.1	6.4 ± 0.5	170.0 ± 20.0	30.0 ± 5.0
Γ_- (C.T.S. 3dP)	0.06 ± 0.01	0.38 ± 0.04	0.08 ± 0.01	0.08 ± 0.01
Γ_+/Γ_- (C.T.S. 3dP)	15.0 ± 3.0	17.0 ± 2.0	2100.0 ± 400.0	380.0 ± 60.0
Γ_+ (C.T.S. 3dI)			140.0 ± 10.0	55.0 ± 5.0
Γ_- (C.T.S. 3dP)			0.1 ± 0.01	0.28 ± 0.05
Γ_+/Γ_- (C.T.S. 3dI)			1400.0 ± 200.0	200.0 ± 40.0
Γ_+^{scaled}				22.0 ± 3.0
Γ_-^{scaled}				0.21 ± 0.05
$\Gamma_+^{scaled}/\Gamma_-^{scaled}$				100.0 ± 60.0
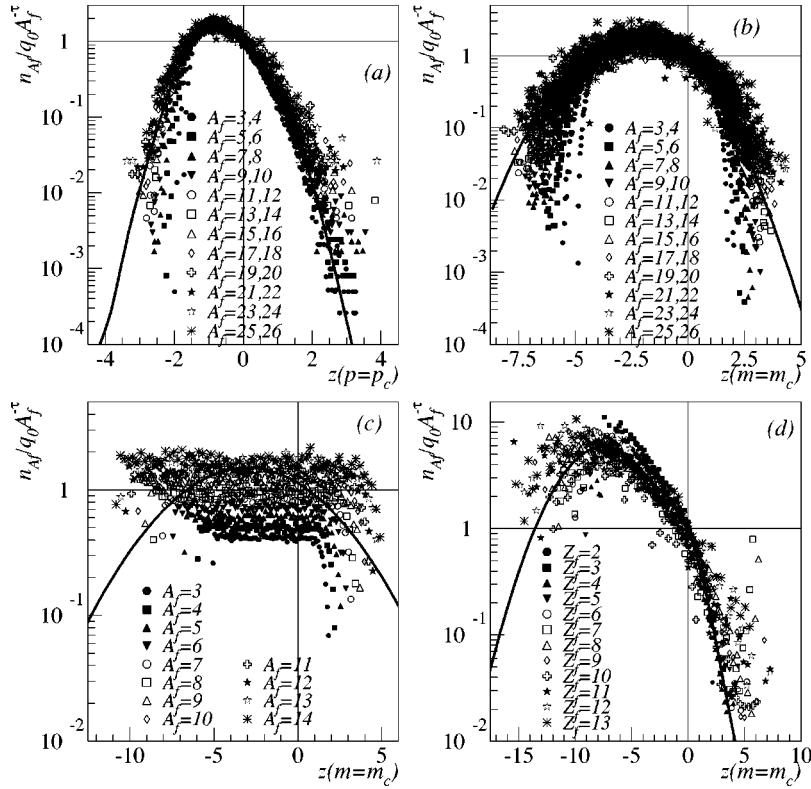
FIG. 19. Results of the scaling function analysis with the critical point equal to the value as determined from the Fisher τ-power law analysis for (a) percolation as a function of $z(p_l)$, (b) percolation as a function of $z(m)$, (c) random partitions as a function of $z(m)$, and (d) Au + C multifragmentation as a function of $z(m)$. Solid curves show the fitted scaling function. See legends for definition of cluster sizes.

the data collapse. In Figs. 19, 20, and 21 error bars on the data points are not shown for the sake of clarity. The size of the error bars reflect the scatter of the data and are larger for larger negative values of z since there were lower statistics for higher multiplicity events [60].

Figure 22 shows a quantitative measure of the data collapse from this scaling analysis. For a number of different choices of control parameter scaling plots, as in Figs. 19–21, were made. Each plot was binned along the abscissa and the rms fluctuations for each bin were calculated. The rms fluc-
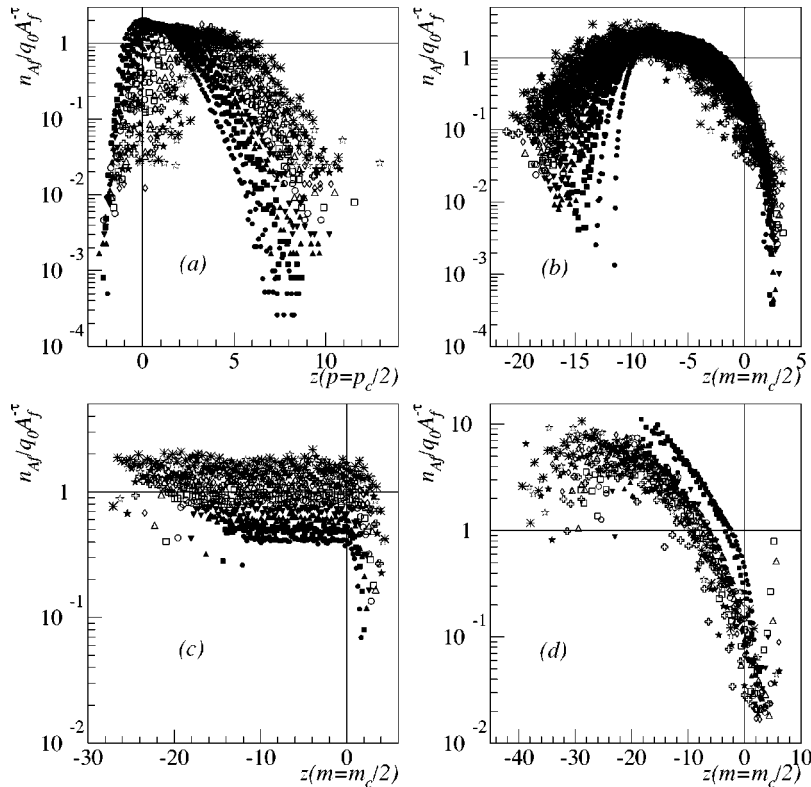

FIG. 20. Results of the scaling function analysis with the critical point equal to half the value as determined from the Fisher τ-power law analysis for (a) percolation as a function of $z(p_l)$, (b) percolation as a function of $z(m)$, (c) random partitions as a function of $z(m)$, and (d) Au + C multifragmentation as a function of $z(m)$. See legends in Fig. 19 for definition of cluster sizes.
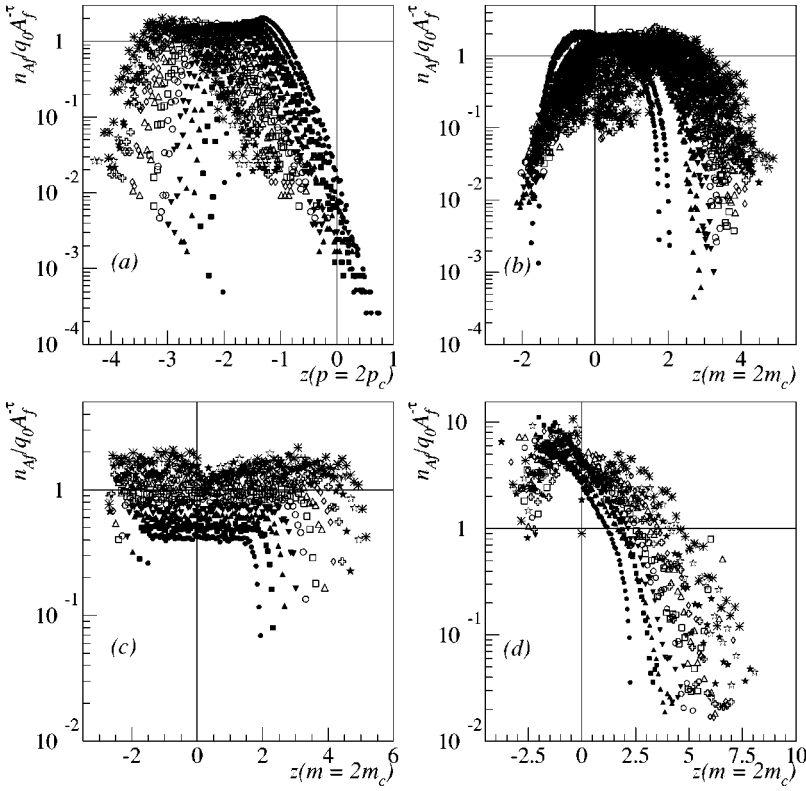
FIG. 21. Results of the scaling function analysis with the critical point equal to twice the value as determined from the Fisher τ-power law analysis for (a) percolation as a function of $z(p_l)$, (b) percolation as a function of $z(m)$, (c) random partitions as a function of $z(m)$, and (d) Au + C multifragmentation as a function of $z(m)$. See legends in Fig. 19 for definition of cluster sizes.

tuations in all bins were then summed and plotted as a function of the choice of critical point, see Fig. 22. In the percolation (p_l and m) and multifragmentation systems the data shows the most collapse in the neighborhood of the Fisher τ-power law critical point. No such behavior is observed in

the random partition system. This analysis serves as another, albeit crude, estimate of the location of the critical point. Table I lists the results.

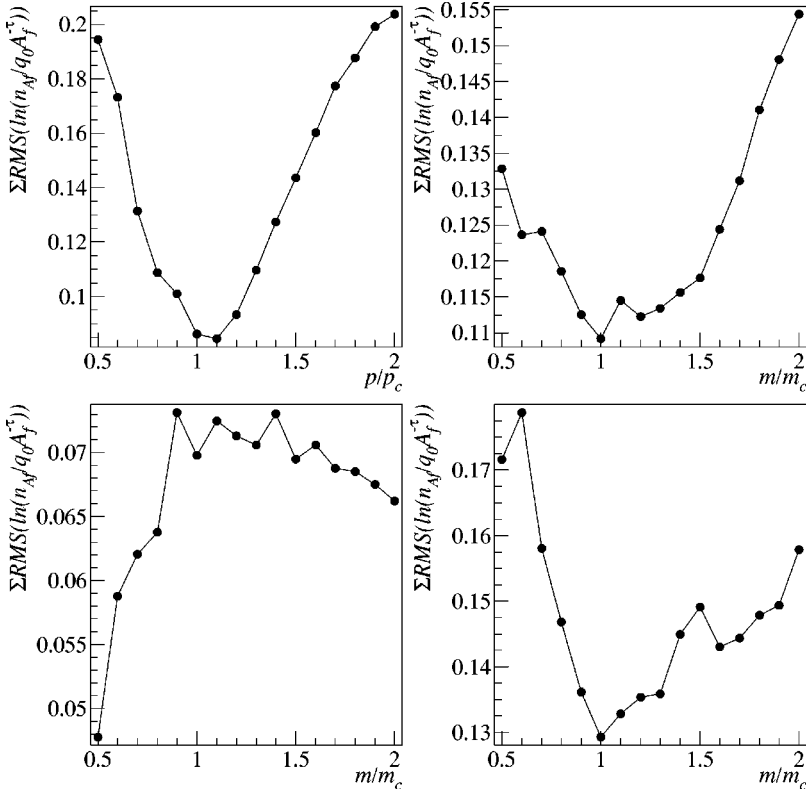The scaled data were used to determine the functional form of the scaling function by fitting the data with an em-

FIG. 22. A measure of the scatter in the scaling function analysis as a function of the choice of the critical point for (a) percolation (p_l), (b) percolation (m), (c) random partitions, and (d) Au + C multifragmentation. Lines are drawn to guide the eye.
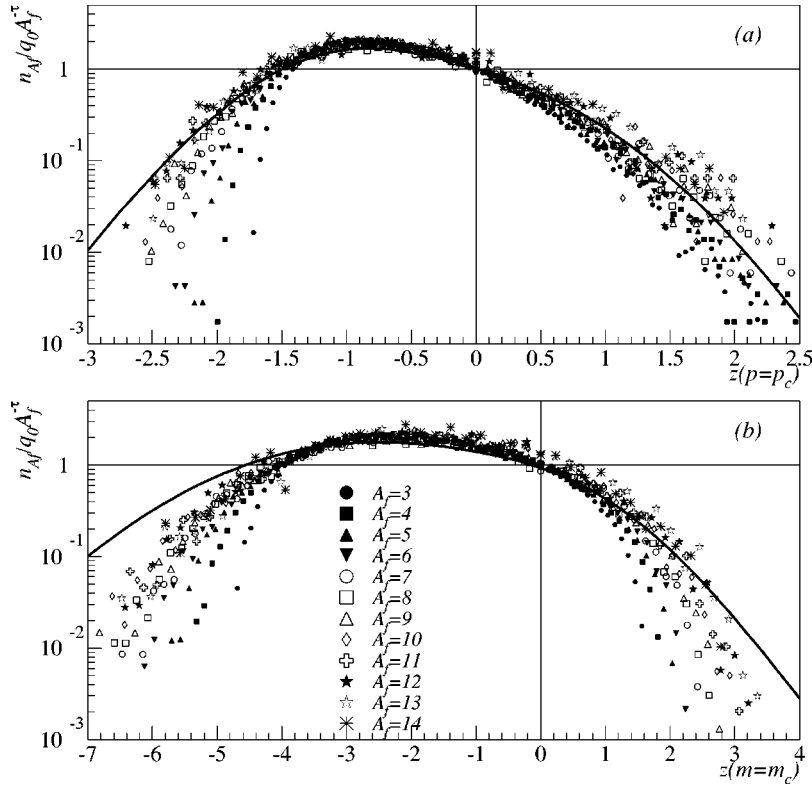
FIG. 23. The scaling function analysis for cluster distribution from a percolation lattice of $A_0 = 64$ as a function of (a) p_l and (b) m. Solid curves show the fitted scaling function from the $A_0 = 216$ lattice. See legend for definition of cluster sizes.

pirical parameterization consisting of two Gaussians instead of the single Gaussian in Eq. (4):

$$f(z) = a_1 \exp\left[-\frac{1}{2}\left(\frac{z-b_1}{c_1}\right)^2 \right] + a_2 \exp\left[-\frac{1}{2}\left(\frac{z-b_2}{c_2}\right)^2 \right].$$

(33)

This was suggested by the asymmetry of the percolation (p_l) data, Fig. 19(a), and is consistent with a simplified version of corrections to scaling [79] as discussed in Sec. V. Figure 19 shows the resulting fits for all systems. Fit parameter values can be found in Table IV. Errors on the parameters of the fits, e.g., a_1, etc., reflect the change in those parameters when the range of clusters included was changed, e.g., clusters with $Z_f = 2$ were included or excluded and so on, and the weighting on the fit was changed, e.g., χ_ν^2 is unweighted, weighted with errors on $n_{A_f}(\epsilon)/q_0 A_f^{-\tau}$ or with errors on $n_{A_f}(\epsilon)/q_0 A_f^{-\tau}$ and ϵ.

The scaling function for percolation (p_l and m) determined here is *the* scaling function for percolation in three dimensions, i.e., it is universal for three-dimensional percolation independent of size. The scaling functions for p_l and m determined above agree well with the scaled cluster distributions of different size lattices, see Fig. 23, and can be used to predict the behavior of the second moment for any size lattice [83]. In the same spirit, the scaling function determined here for gold multifragmentation is *the* scaling function for charged nuclear matter which describes the cluster distributions produced in the multifragmentation of any nucleus, not just the excited gold remnant discussed in this work. With the knowledge of the form of the scaling function various other quantities can be determined as illustrated in Sec. III and shown below.

The cluster distributions for the random partitions is fit, by eye, with the same empirical parametrization as in Eq. (33) see Fig. 19(c). The random partitions cannot be described by Eq. (33). The solid curve in Fig. 19(c) will be used in the following section to demonstrate the failure of the scaling analysis, as is also seen here, when applied to a system where a continuous phase transition is absent. Fi-

TABLE IV. Scaling function parameters.

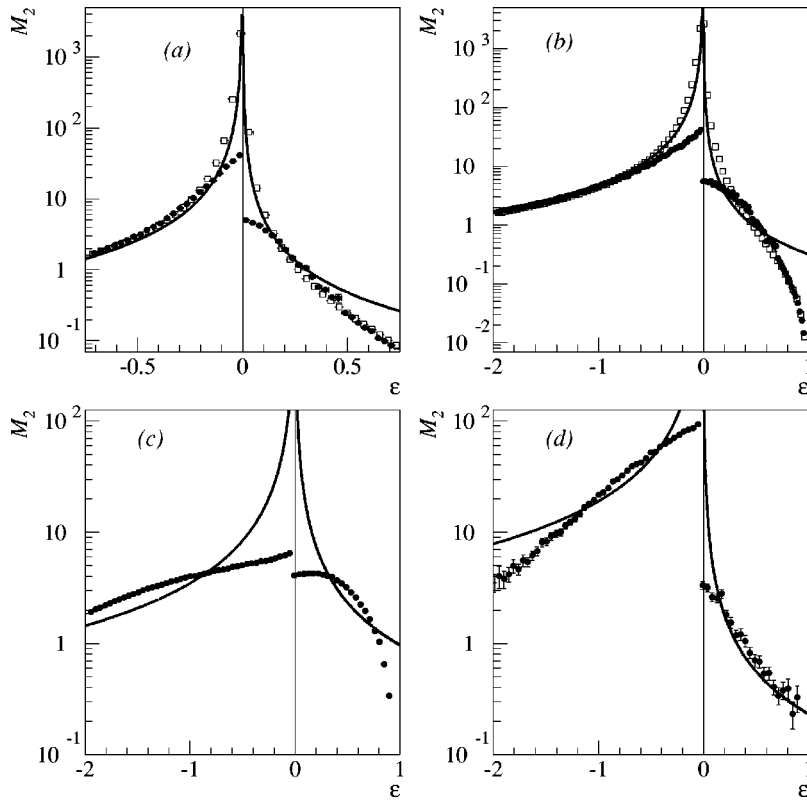| Parameter/system	Percolation (p_l)	Percolation (m)	Random partitions	Au + C	Scaled Au + C
a_1	0.8±0.2	1.8±0.2	0.75±0.5	5.9±0.1	2.0±0.2
b_1	−1.0±0.1	−2.6±0.3	−3.0±0.5	−7.5±0.3	−3.0±0.3
c_1	0.5±0.2	1.8±0.2	4.0±0.5	3.2±0.1	2.1±0.2
a_2	1.0±0.1	0.3±0.03	0.75±0.5	0.8±0.2	6.3±0.7
b_2	−0.5±0.1	0.1±0.01	−3.0±0.5	−1.2±0.4	−10.0±1.0
c_2	0.8±0.2	1.1±0.1	4.0±0.5	1.5±0.2	3.3±0.4

FIG. 24. Results of the γ-power law determined from the scaling function for (a) percolation (p_l), (b) percolation (m), (c) random partitions, and (d) Au + C multifragmentation. Solid lines show the γ-power law predicted from the scaling function σ and τ. Filled circles show the second moment as a function of ϵ. Open squares in (a) and (b) show the second moment behavior of a percolation lattice of size $A_0 = 250,047$.

nally, a consistency check in this analysis is the agreement between the location of the peak in the scaling functions and the values of z_{max} determined in the σ analysis, see Table III.

4. γ-power law from the scaling function

The behavior of κ_T or M_2 can be *derived* from the functional form of the scaling function and the critical parameters via Eq. (17). Performing the integration in Eq. (17) using the functional form of the scaling function determined above yields a direct calculation of the critical amplitudes $\Gamma_\pm$ via Eq. (19). The critical exponent γ is calculated from the values of τ and σ via a scaling relation in Eq. (18). Combining these two, $\Gamma_\pm$ and γ, it is possible to calculate the γ-power law that describes the behavior of the second moment. This calculated γ-power law can then be compared to the behavior of M_2 as measured from the cluster distribution. Figures 24(a), 24(b), and 24(d) shows the agreement between the measured M_2 data (largest cluster omitted in the liquid region) and the calculated γ-power law curves for percolation (p_l and m) and gold multifragmentation, respectively, and Tables II and III list the results.

The values of γ determined via the scaling relation in Eq. (18) for percolation (p_l and m) show approximate agreement with the accepted value of 1.8. The high value of σ extracted above leads to a low value of γ here. Figures 24(a) and 24(b) also show the behavior of the second moment of a 250,047 site lattice. The power law predicted using the scaling function determined with a 216 site lattice shows rough agreement with the measured M_2 of the larger lattice in both the amplitude ($\Gamma_\pm$) and exponent (γ). There is approximate agreement between the predicted power law and the mea-

sured M_2 of the smaller lattice over some region in ϵ that is neither too near to, nor too far from the critical point, $\epsilon=0$. It is this region that will be determined, independently, in the following section.

For the percolation (p_l and m) system, the disagreement between the measured M_2 data and the calculated curves is due to two well-known reasons: far from the critical point, the assumptions of scaling are no longer valid and the analytic background overwhelms the singular behavior. Near the critical point finite size effects dominate M_2, limiting the sizes of the large clusters which make the most significant contribution. In contrast, the τ-power law was observed at the critical point because it is determined by smaller clusters which suffer the least from the finite size effects.

Figure 24(c) shows the results when this analysis was applied to random partitions. The power law predicted from the scaling function analysis applied to the cluster distribution of the random partitions fails to reflect the behavior of the measured second moment. This is not surprising as the random partitions presented here are not the result of a system undergoing a continuous phase transition. The disagreement observed in Fig. 24(c) then serves as an indication of how this particular analysis probes for the presence of a continuous phase transition. This figure shows the results of this analysis for a system with no phase transition, while Figs. 24(a) and 24(b) show the results of this analysis on a system where such a phase transition is present.

The results of this analysis when applied to nuclear multifragmentation are shown in Fig. 24(d). In this case, the comparison to the predicted γ-power law is neither as good as that for percolation nor as poor as that for the random

partitions. It shall be shown in Sec. VI that some improvement can be achieved if account is taken of the changing system size $A_0(m)$ and finite size scaling effects.

The approximate agreement between the predicted γ-power law and the measured M_2 behavior is in keeping with the behavior expected for small systems undergoing a continuous phase transition, e.g., the percolation system. The multifragmentation results are clearly different that then results of a system without a continuous phase transition, e.g., random partitions.

5. γ matching

In the previous works the procedure for determining critical exponent values and the location of the critical point from the cluster distribution was based on a method of matching exponent values on both sides of the critical point [12,71]. The idea was to find the region on either side of the critical point where the power law behavior predicted by the scaling function holds. As is seen in Fig. 24 there is some intermediate ϵ region where the second moment data are described by a power law, a region where the M_2 behavior is dominated by the γ-power law and all other effects are small in comparison. In earlier percolation studies [71] general guidelines based on the correlation length and size of the fluctuations were used to find the boundaries in ϵ of the regions to be fit. In nuclear multifragmentation analyses [12] it was impossible to use such guidelines. Instead a method was developed that searched for regions best fit by power laws and determined the location of the critical point and exponent values simultaneously. The values of the critical exponents and the normalizations associated with power laws were obtained from the best fit power laws in those regions. As with the previous analyses presented in this paper, this method of exponent matching does not select a particular value of a critical exponent or the critical point. Instead the values found are the outcome of an unbiased procedure.

The method is as follows. A choice of the critical point, p_c or m_c was made. From this choice plots such as those shown in Fig. 24 were made. Then fitting boundaries in ϵ were chosen. The fitting range was defined by $\epsilon_{\pm}^{\text{far}}$ and $\epsilon_{\pm}^{\text{near}}$. For example, on the gas side of the critical point a fit of $\ln(M_2)$ versus $\ln(|\epsilon|)$ was made for all data with $|\epsilon_+^{\text{near}}| \leqslant |\epsilon| \leqslant |\epsilon_+^{\text{far}}|$. The slope of the resulting linear fit was recorded as γ_+, the offset as $\ln(\Gamma_+)$ and the goodness of fit as $\chi^2_{\nu+}$. The same procedure was applied to the liquid side of the chosen critical point, recording γ_-, $\ln(\Gamma_-)$, and $\chi^2_{\nu-}$. For each choice of the critical point, several choices of fitting regions $\epsilon_{\pm}^{\text{far}}$ and $\epsilon_{\pm}^{\text{near}}$ were made and results recorded. Five parameters were chosen for each region examined: $\epsilon_{\pm}^{\text{far}}$, $\epsilon_{\pm}^{\text{near}}$, and p_c or m_c.

The fit regions and critical point locations were evaluated by demanding that (1) they yield γ_+ and γ_- values that matched each other to within the error bars on those values returned by the fitting routine and (2) that the χ^2_{ν} of the fits were in the lowest quarter of the distribution resulting from all the fits which satisfy condition (1). The results from the power law fit regions that passed these two criteria were then

histogrammed and average values for all quantities concerned were determined. The results are summarized in Tables I, II, and III and shown in Fig. 25.

The lines plotted in Fig. 25 do not result from any single fit, but display the average results for $\gamma_{\pm}$ and $\Gamma_{\pm}$ that have satisfied conditions (1) and (2). The points in Fig. 25 are the measured second moment for the particular cluster distribution in questions plotted against ϵ, which depends on the average value of p_c or m_c that satisfies conditions (1) and (2). Therefore the lines in Fig. 25 should not be interpreted as a fit to the data points shown, but as the average results from the γ-matching procedure. Full circles in Fig. 25 show the average fitting regions that satisfy conditions (1) and (2).

For percolation p_l the value of γ determined in this manner is within a few percent of the value determined in Ref. [71] and the infinite lattice value. The ratio of Γ_+/Γ_- determined by this method, a ratio that depends on the universality class of the system in question, is also in agreement with the infinite lattice value and the $\Gamma_{\pm}$ values predicted by the scaling function, see Table III. The value of p_c determined here is within 15% of the value determined in a previous analysis of the $L=6$ lattice [71] and the value determined above in the Fisher τ-power law analysis, see Table II and Fig. 25(a).

The results for the analysis of percolation with m as a measure of the control parameter are worse that the results when the natural control parameter p_l is used, the difference in γ_+ and γ_- was $\Delta\gamma^m = 0.06 \pm 0.1$ compared to $\Delta\gamma^{p_l} = 0.0 \pm 0.3$. This is to be expected because for each value of p_l there is some spread in the resulting values of m, so that binning in m groups together *events* with different values of p_l. There is also a nonlinear relation between the average values of p_l and m [83]. In spite of these two effects the results of the analysis in Sec. IV B 4 suggests that vestiges of the signature of a phase transition are still present even when m is used as the control parameter. That is also the case in the present analysis. Table II shows that the γ value agrees, within error bars, with the infinite lattice value. The values of the critical amplitudes $\Gamma_{\pm}$ do not yield a ratio that agrees with the infinite lattice value. This is due to the non-linear mapping of p_l onto m and is discussed in Ref. [83].

When the γ-matching procedure was applied to the cluster distributions from random partitions a very limited amount of trial fits passed the combined tests of (1) and (2). The results compared poorly to the percolation results. At best the values of γ_+ and γ_- match to within 20% of the average value of γ, compared to perfect matching for percolation p and matching within 5% for percolation m. The value of the critical point m_c returned from this analysis also compared poorly to other outcome of previous analyses, see Table I. Finally, while fit regions for all systems were limited, the fit regions are the smallest for the random partitions.

The results of the γ-matching analysis applied to multifragmentation data has been published in Ref. [12]. In that work the data were contaminated by the inclusion of prompt nucleons; prompt nucleons are excluded from consideration in this work. In that work the second moment of the cluster distribution was determined based on the charge of a cluster rather than its mass as is done in this work. Previously, the
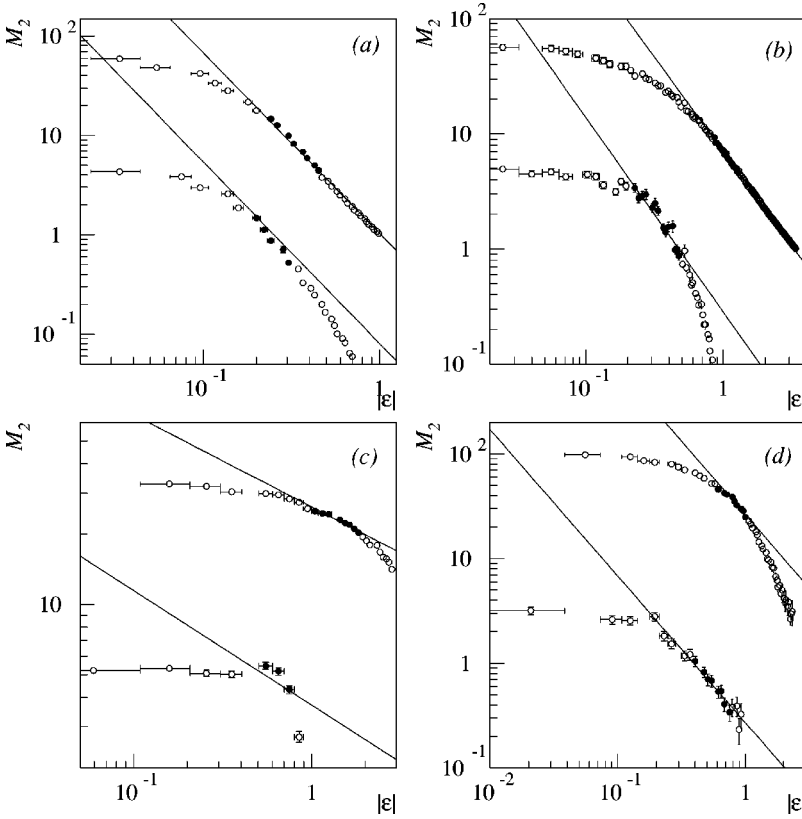
FIG. 25. Results of the γ-matching analysis for (a) percolation (p_l), (b) percolation (m), (c) random partitions, and (d) Au + C multifragmentation. Solid lines show the average γ-power fit returned by the procedure. Open circles show the entire second moment behavior, filled circles show the average fitted region returned by the procedure. See text for details.

second moment was generated from a cluster distribution that was not normalized to the changing size of the system as is done here. Furthermore the prior analysis consisted of only one quarter of the total number of events used in the present analysis. Thus the current analysis has higher statistics, has been freed of prompt nucleons, has a second moment that has been constructed with the masses from the cluster distribution and a cluster distribution that has been normalized to the changing system size. The exclusion of prompt nucleons and normalization to the changing system size are an effort to address the criticisms raised in Ref. [84] and rebutted in Ref. [85]. When the γ-matching procedure was applied to the data presented in this paper essentially the same results as presented in Ref. [12] were recovered. See Table II and Fig. 25(d). One difference observed is in the value of the critical point returned, $m_c^{94}=26\pm1$ reported in Ref. [12] and $m_c^{99}=21\pm2$ reported in this work. The difference is not as great as it appears to be. The origin of the published value of m_c^{94} lies in picking the peak of the distribution of m_c values that satisfied conditions (1) and (2) as the location of the critical point. The value was estimated based on the location of the maximum and the error based on the width of the distribution in m_c. The mean and rms of the m_c distribution in Ref. [12] suggest a value of the critical point of $m_c^{94}=25\pm3$. This value agrees, to within error bars, with the value of m_c^{99} presented here. The relatively small shift in m_c can then be understood to arise from the differences in the data sets. Noting this it is clear that the present γ-matching analysis is in agreement with the previous work.

The results of the present work are, again, in keeping with the expected results of a small system undergoing a continu-

ous phase transition. There is some region where matching γ values can be obtained, some regions in ϵ where the γ-power law overwhelms all other effects. The fits in Fig. 25(d) are of higher quality than those for random partitions in Fig. 25(c) and cover a greater range. When compared to the percolation m results the multifragmentation data compare favorably in terms of overall goodness of fits, width of fit region and matching of $\gamma_\pm$, see Table II. The location of the critical point returned by this analysis also compares well with the location from other analyses, see Table I.

V. CORRECTIONS TO SCALING

In the last section it was seen that the γ-power law and the data for the second moment in all systems agreed over only a limited area. To some degree this is to be expected. Near the critical point, assumptions valid for thermodynamic systems are invalid for the finite systems discussed in this work. For that reason, finite size effects dominate at the critical point and the second moment peaks instead of diverging. Far from the critical point other effects come into play. The scaling assumptions inherent in the FDM are valid only in the neighborhood of the critical point. The size of this neighborhood is somewhat ill defined and seems to depend on many factors, e.g., the quantity in question, the nature of the system, the size of the system and so on.

However, scaling behavior in physical systems can be observed over a wide range in temperatures and densities. This is most elegantly illustrated in the Guggenheim plot [86] of scaled temperature (T/T_c) as function of scaled density (ρ/ρ_c) for several different gases (Ne, Ar, Kr, Xe, N$_2$, O$_2$,

CO, and CH_4). In that plot the data collapse onto a curve that is well described by a power law with an exponent of $\beta = 1/3$. The range in validity of this agreement between data and power law is shown on the Guggenheim plot to be over a range of $\Delta T \sim 0.5 T_c$ and $\Delta \rho \sim 2.5 \rho_c$. However, another system, the combination of isobutyric acid and water, shows the Guggenheim type of scaling only near the critical point [87]. Already when the range considered is $\Delta T \sim 0.04 T_c$ and $\Delta \rho \sim 0.01 \rho_c$ corrections to scaling can be observed. To that end, higher order corrections to scaling are now examined in order to determine if fits such as those shown in previous sections can be improved. However, improvement comes at the expense of more fit parameters and assumptions.

To fully explore corrections to scaling in the context of the present systems where the cluster distributions serve as the main observable the FDM is revisited in a fashion employed in Refs. [79,88]. Assuming coexistence Eq. (6) is then rewritten as

$$n_{A_f}(\epsilon) = q_0 A_f^{-\tau}[f_0(z) + A_f^{-\Omega} f_1(z) + \cdots], \qquad (34)$$

where $f_1(z)$ is the correction-to-scaling function and Ω is the correction-to-scaling exponent. The form of Eq. (34) anticipates the presence of a second function of z. In Sec. IV 3 it was found empirically that both the scaled percolation and multifragmentation cluster distributions $[n_{A_f}(\epsilon)/q_0 A_f^{-\tau}]$ could be reasonably well described by the sum of two Gaussians, Eq. (33). In that treatment, the amplitude of each gaussian was a constant, a_1 and a_2. If A_f is restricted to a single value, the prescription give by Eq. (34) is equivalent to that of Eq. (33). Equation (34) predicts that there should be an ordering to the scaled cluster distributions, i.e., smaller cluster sizes should lie above the larger clusters due to the correction term. This can be observed in Figs. 19(a) and 19(b) in the neighborhood of the maximum of the scaled data for the percolation systems. In the tails of the distribution, either large or small cluster production is suppressed. In the case of multifragmentation data, Fig. 19(d), the ordering is generally observed where the statistics are adequate, namely, near $z = 0$. The ordering of the random partitions implies that $\Omega < 0$.

From Eq. (34) it possible to derive the *corrected* isothermal compressibility (second moment) power law. Following the method in Sec. III leads to

$$\kappa_T \sim (\rho^2 k_b T)^{-1} \left(\left| \frac{q_0}{\sigma} \int_0^{\pm\infty} dz f_0(z) \right| z \right|^{(3-\tau-\sigma)/\sigma}$$

$$\left. \left| + \left| \frac{q_0}{\sigma} \int_0^{\pm\infty} dz f_1(z) \right| z \right|^{(3-\tau-\sigma-\Omega)/\sigma} \right| \epsilon \Big|^{\Omega/\sigma} \right) |\epsilon|^{\tau-3/\sigma}$$

$$(35)$$

which is usually simplified and written as

$$\kappa_T \sim \Gamma_{\pm} |\epsilon|^{-\gamma} (1 + a_{\pm} |\epsilon|^{\Delta}). \qquad (36)$$

Now the overall amplitude, $\Gamma_{\pm}$ is given by the first integral, and the correction-to-scaling amplitude is given by the sec-

ond integral divided by the first. The correction-to-scaling exponent is $\Delta = \Omega/\sigma$.

Using Eq. (36) to fit the second moment distribution would lead to determining four fit parameters: two amplitudes and two exponents. To explore the effects of corrections to scaling an assumption was made as to the universality class of the system in question and thus the choice of exponent values. For the three-dimensional percolation universality class $\Delta = 1.22$ [79,88] and for the three-dimensional Ising universality class $\Delta = 0.56$ [89–91]. The amplitudes were left as free parameters and the second moment of the cluster distributions were fit. The value of the critical point determined from the γ-matching analysis of Sec. IV B 5 was used for each system. Figure 26 shows the results.

For the percolation system with the corrections-to-scaling a better fit to the second moment data was possible over a range in ϵ up to twice the range of the average fitted region in the γ-matching analysis, see Figs. 26(a) and 26(b). The fits still failed to reproduce the behavior of M_2 near the critical point where finite size effects dominate the system. Table III lists the results for the critical amplitudes $\Gamma_{\pm}$. The agreement in the critical amplitudes determined in this analysis and the amplitudes from the γ matching analysis is due to the agreement of the behavior of Eq. (36) and the γ-power law from the γ-matching analysis over the region in ϵ determined by γ-matching. Thus the γ-matching analysis finds regions that are the least affected by higher-order corrections to scaling.

For the random partitions an improvement is only observed for the high multiplicity region where a better fit over a larger range was obtained for both choices of universality class, see Fig. 26(c). The low multiplicity events showed no such improvement partly due to the limited range in ϵ available. Both the three-dimensional percolation and three-dimensional Ising exponents were used in this analysis for the random partitions and the multifragmentation data. Both choices of universality classes showed similar results. The lack of effect of corrections to scaling is to be expected in a system that does not follow FDM-like scaling laws.

The multifragmentation data also showed improvement resulting in a better agreement between the fits and the M_2 data points over a larger range in ϵ, see Fig. 26(d). The improvement was observed for both choices of universality classes thus indicating this analysis is insensitive to the differences [92,93], though the goodness of fit was better for the choice of the three-dimensional Ising exponents over the same fit regions (3D Ising: $\chi^2_{\nu+} = 0.4$ and $\chi^2_{\nu-} = 0.7$; 3D percolation: $\chi^2_{\nu+} = 0.7$ and $\chi^2_{\nu-} = 1.1$). At this level of analysis it appears that corrections to scaling improves the fits for the γ-power law. Whether this is due to the presence of a continuous phase transition in nuclear multifragmentation, or merely extra terms in the fitting function remains an open question.

VI. CHANGING SYSTEM SIZE AND FINITE SIZE CORRECTIONS

It has been pointed out that the previous statistical analysis of gold multifragmentation [12] ignored the changing size of the system [84]. To first order this may have been a reasonable procedure [85] as many statistical signatures of a
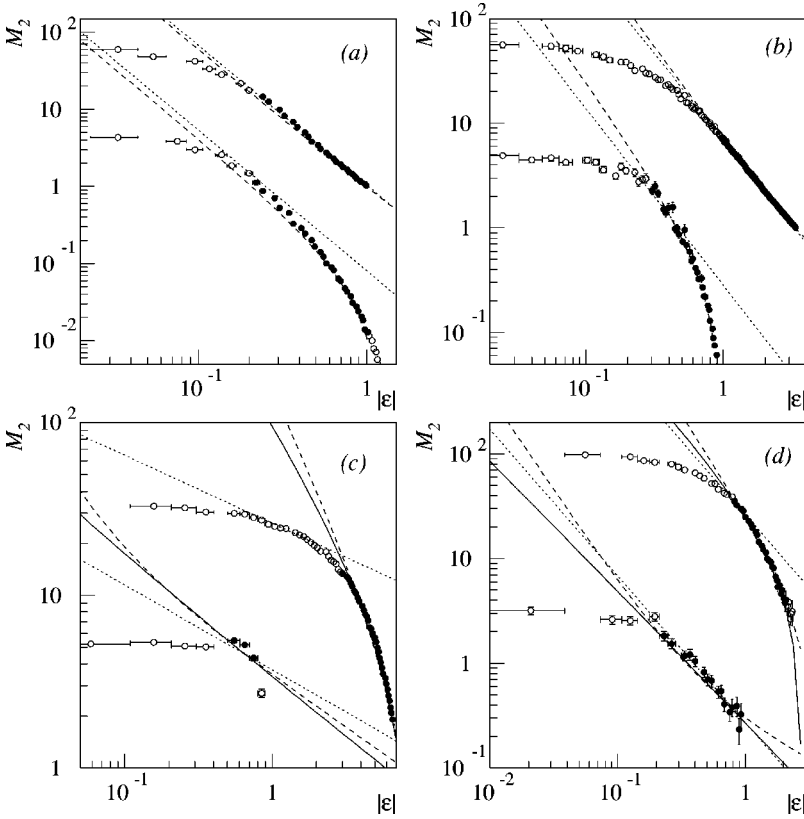
FIG. 26. Results of the correction-to-scaling analysis for (a) percolation (p_l), (b) percolation (m), (c) random partitions, and (d) Au + C multifragmentation. Open circles show the entire second moment behavior, filled circles show the fitted region used in this procedure. See text for details. Dotted lines show the γ-matching power law. Dashed (solid) lines show the resulting correction-to-scaling γ-power law for the 3D percolation (3D Ising) universality class.

continuous phase transition have been observed both before and after the scaling to account for the changing system size has been performed; e.g., the γ power law shown here and in previous works agree well. However, the data collapse in Fig. 19(d) is qualitatively not as great as that shown by the percolation (m) system in Fig. 19(b) and the agreement between the calculated and measured M_2 behavior in gold multifragmentation in Fig. 24(d) is qualitatively not as good as that shown by percolation (m) in Fig. 24(b). In this section, the effect of the changing size of the system is explored and accounted for.

The size of the multifragmenting system is shown in Fig. 27(a) after Ref. [60]. An approximately linear relation between the system size A_0 and m was found: $A_0 = 199 - 1.6m$, see Fig. 27(a). The functional form of $A_0(m)$ was used in the following analysis to account for the changing system size in an average way, i.e., not on an event-to-event basis.

If the multifragmenting system is assumed to be a system undergoing a phase transition, then the theory of finite size scaling of the critical point [94–97] suggests that the effective critical temperature $T_c(A_0)$, changes as a function of the system size. Coupling this with the changing size of the system indicates that at each value of m the value of $T_c^{eff}(A_0)$ is different.

The value of $T_c^{eff}(A_0)$ can be determined in the following manner. First a relation between the multifragmenting system's temperature T and m must be determined. Again from Ref. [60] a relation can be found, see Fig. 27(b). Two estimates of T were made, one from a Fermi gas (uncorrected for the effect of expansion energy) T_i and the other from an

isotopic yield ratio thermometer T_f [98]. These temperatures give an approximate indication of the initial and final temperatures of the system. Figure 27(b) shows that T_i is well fit by a quadratic function, while T_f is well fit by a linear function. Another linear function reproduces the average of T_i and T_f: $T = 3.0 + 0.14m$, this was used for the following analysis. The critical temperature of infinite nuclear matter was assumed to be $T_c^\infty = 22.9$ MeV [99].

From the Fisher τ-power law analysis the value of the multiplicity at the critical point was determined to be $m = m_c = 22 \pm 1$. The system size at that point is then $A_0(m = 22) = 164 \pm 2$ and the temperature is $T = 6 \pm 2$ MeV. This indicates that the critical temperature for a charged nuclear system with 164 nucleons, $T_c^{eff}(A_0)$, is approximately 6 ± 2 MeV.

According to theory, to first order the critical point scales with system size as

$$[T_c^{eff}(A_0) - T_c^\infty]/T_c^\infty = bA_0^{-1/d\nu}, \tag{37}$$

where d is the Euclidean dimension of the system and ν is the so-called hyperscaling exponent. At the smallest of system sizes higher order correction terms may play an important role in the scaling of the critical point [100]. This formalism is usually applied to neutral matter. Obviously the excited nuclear system dealt with in this work is charged. In an attempt to account for the effects of the Coulomb force felt by the nuclear system $T_c^{eff}[A_0(m = 22)]$ was increased by adding $0.25 + 0.016A_0(m)$, in keeping with the work of Ref. [99] regarding the effects of the Coulomb energy on the critical temperature. For $A_0 \sim 164$, $T_c^{eff} \sim 9$ MeV.
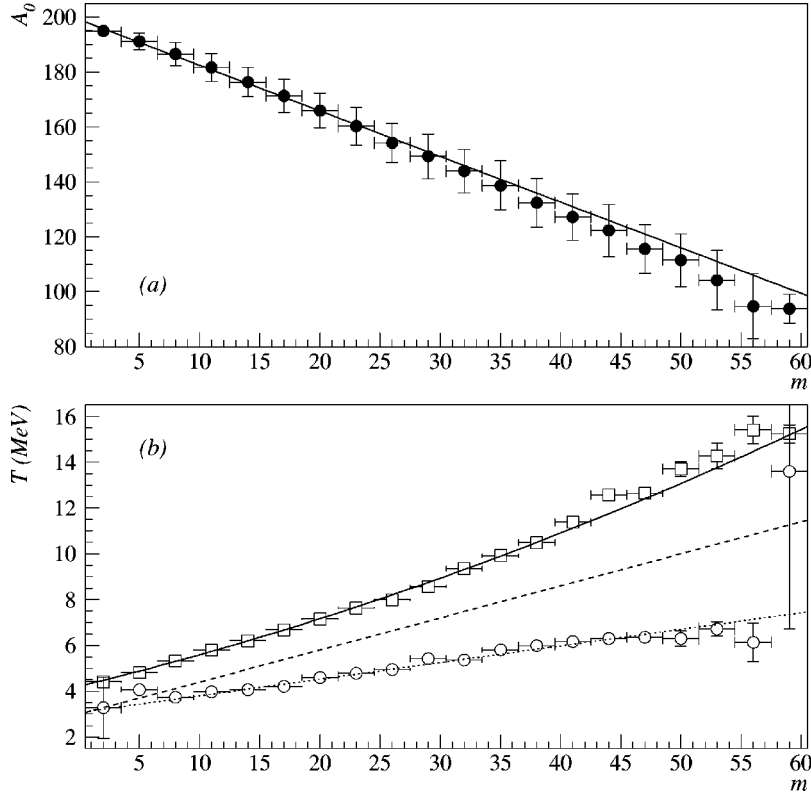
FIG. 27. (a) Behavior of the size of the system, A_0, with respect to the total charged particle multiplicity, m. The solid line is a fit to the changing system size. (b) measures of the temperature T as a function of m: $\square$ T_i from a Fermi gas and $\bigcirc$ T_f from an isotope thermometer. The solid curve shows a fit to T_i, dotted curve a fit to T_f, and the dashed curve a fit to $\langle T \rangle = (T_i + T_f)/2$.

If it is assumed that gold multifragmentation is the result of a continuous phase transition and that transition occurs in three dimensions, $d = 3$, then using the hyperscaling relation [61]

$$\nu = \frac{\tau - 1}{d\sigma}, \qquad (38)$$

with the extracted values of σ and τ, gives $\nu = 0.63 \pm 0.07$. The coefficient b in Eq. (37) can be determined using $T_c^{\mathrm{eff}}[A_0(m_c)] = 9 \pm 2$ MeV, T_c^{∞}, d, and ν; resulting in $b = -9 \pm 2$. Note that this value of b suggests that $T_c^{\mathrm{eff}}(A_0) = 0$ for $A_0 = 60 \pm 40$. This is a result of the form of Eq. (37) and the notion that the critical temperature lowers as the size of the system decreases. Presumably higher order effects not taken into account in Eq. (37) will affect the location in system size, A_0, where the effective critical temperature vanishes. For the form of finite size scaling corrections shown in Eq. (37), only $b = -1$ yields an effective critical temperature that vanishes at $A_0 = 1$.

Now Eq. (37) can be used to solve for $T_c^{\mathrm{eff}}[A_0(m)]$, this measure of the effective critical temperature is for neutral material. To account for the effects of the Coulomb energy present in a nuclear system this estimate is lowered by $0.25 + 0.016A_0(m)$. The scaled control parameter is then

$$\epsilon^{\mathrm{scaled}} = \{T_c^{\mathrm{eff}}[A_0(m)] - T\}/T_c^{\mathrm{eff}}[A_0(m)]. \qquad (39)$$

The analysis to extract the exponent σ was performed with this $\epsilon^{\mathrm{scaled}}$ by finding the peak in A_f sized cluster production as a function of $n_{A_f}(\epsilon^{\mathrm{scaled}})$ versus $\epsilon^{\mathrm{scaled}}$. Previously, it was argued that the largest cluster should be excluded for

all values of ϵ to account for finite size effects in the analysis to extract σ. The analysis in this section directly accounts for finite size effects, thus the standard FDM formalism with respect to the largest cluster is followed. This results in a value of $\sigma = 0.65 \pm 0.07$ and $z_{\mathrm{max}}^{\mathrm{scaled}} = -10 \pm 2$, Fig. 28(a) shows the resulting power law.

The scaling function for gold multifragmentation was then plotted using the above corrections for the changing system size and finite size scaling, see Fig. 28(b). The data collapse is qualitatively better than in Fig. 19(d). The two gaussian parametrization of $f(z^{\mathrm{scaled}})$ was fit to the scaled scaling function and is shown in Fig. 28(b) with parameters listed in Table IV.

Using the fitted parametrization of the scaling function and other quantities, the γ-power law can be determined as before. Figures 28(b) and 28(c) show the measured M_2 of gold multifragmentation plotted as a function of $\epsilon^{\mathrm{scaled}}$. A γ-power law was plotted on, not fitted, Figs. 28(b) and 28(c) with $\gamma = 1.3 \pm 0.2$ [from τ, σ and Eq. (18)] and offsets determined via the scaled scaling function. This γ-power law agrees moderately well with the measured M_2 the full $\epsilon^{\mathrm{scaled}}$ range, the exception being near $\epsilon^{\mathrm{scaled}} = 0$ where finite size of the system limits the maximum of M_2. The treatment of the effects of the Coulomb energy in this analysis is model dependent. However, if the Coulomb effects are completely neglected, the results are unchnaged to within error bars.

VII. DISCUSSION AND CONCLUSIONS

The focus in the present paper was on the behavior of cluster distributions and the types of analyses which can shed light on their creation mechanism. In particular, attempts were made to identify procedures that can distinguish those
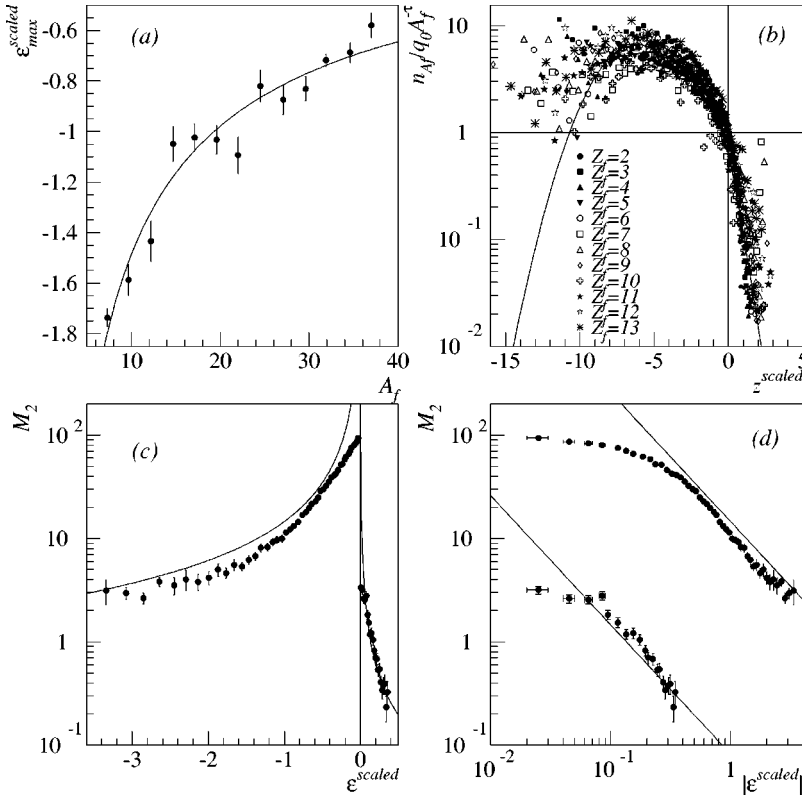
FIG. 28. Results of the system size / finite size scaling analysis for Au + C multifragmentation. (a) The scaled σ power law. (b) The scaling function, normalized cluster distribution versus z^{scaled}. The solid curve shows the fitted scaling function. See legend for definition of cluster sizes. (c) and (d) show the resulting γ-power law as predicted from the scaling function, σ and τ. Solid circles show the second moment plotted against the properly scaled ϵ^{scaled} and solid lines show the predicted γ-power law.

distributions which are related to critical behavior from those which are not. While this question is easily answered for systems containing large numbers of constituents, it is more difficult to address the case of interest here, namely, systems with at most only a few hundred particles. In order to answer this question for small systems, two different computational models, bond building percolation and a random partitions, have been used. It is well known that in the macroscopic limit, the former system possesses a continuous phase transition characterized by a unique scaling function and set of critical exponents while the latter system does not. In addition, data arising from the multifragmentation of gold nuclei has been studied using the same procedures. For this system, it is not known, *a priori*, whether a critical point is present.

Many cluster properties have been proposed as being suitable measures of critical behavior. Among these are the fluctuations in the size of largest fragment (Fig. 1), peaking in the quantity γ_2 (Fig. 3), peaking behavior in M_2 (Fig. 5), Campi plots (Fig. 6) and simple power law behavior in the cluster mass distribution for a particular value of the appropriate control parameter. It was seen that none of these measures, taken alone or together, was sufficient to distinguish a system possessing critical behavior from one which does not.

The first procedure which produced different results for critical and noncritical systems was the single parameter power law fit to the cluster mass distribution (Figs. 12–15). For the percolation systems and for the multifragmentation data, it was shown that the one parameter power law fit describes the data well only over a very limited range of the control parameter. The value of the control parameter where the power law fit is best is very close to where the above-

mentioned peaks occur. For the random partitions, this was not the case.

If a system possesses a critical point, it is also expected to possess a scaling function that describes its behavior away from the critical point. Phase transition theory specifies how the argument of this function depends on cluster mass and distance from the critical point. If such a function exists, the theory permits the determination of the critical exponent σ. This determination was done for the percolation system yielding satisfactory agreement with its known value. The same procedure was applied to the random breakup model and to the multifragmentation data. It was clear from this analysis that percolation and multifragmentation were similar in many features, while the random system was different, see Figs. 17 and 18.

Again, if a system possesses a critical point, it is expected to possess a scaling function that describes its behavior away from the critical point. Therefore, when the data is properly scaled, it should collapse onto a single curve. Figure 19 shows the amount of data collapse for the systems discussed here. The quality of the data collapse (Figs. 19–21) reinforces the notion that the random breakup system is different from the others. Although the precise form of the scaling function is not dictated by phase transition theory, both the percolation system and multifragmentation data were satisfactorily described by a sum of two Gaussians. The random breakup model was not.

The issue of finite size scaling was discussed. Unlike the other systems examined here, which had a fixed number of constituents, the nuclear multifragmentation data originated from systems whose size varied monotonically with observed charged particle multiplicity, see Fig. 27(a). Phase transition theory makes a prediction, Eq. (37), as to how the
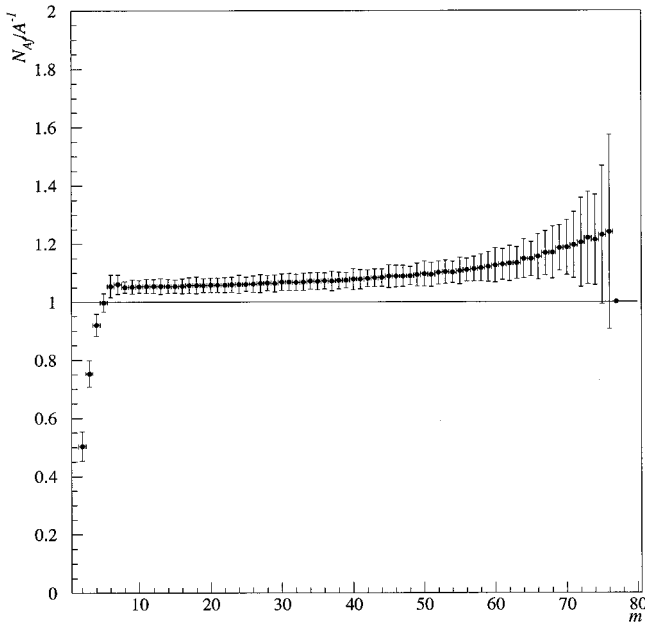
FIG. 29. Results of a scaling analysis performed on the cluster distribution of random partitions. The scaled cluster distribution (nearly) collapses to unity over the entire multiplicity range.

FIG. 30. Results of the summation to determine the offset q_0 as a function of the upper limit of the summation.

value of the control parameter at the critical point changes as a function of system size. Applying Eq. (37) produced an improvement in the quality of the data collapse for the scaling function and yielded a better prediction for the behavior of M_2, see Fig. 28.

Critical exponent values have been determined in an unbiased manner for each system. For both sets of analyses on the percolation clusters, the standard percolation exponents were recovered to within error bars. For the random partitioning, exponents could be extracted, but none that fulfilled well known scaling laws. The exponent values determined from the gold multifragmentation cluster distributions fulfill the scaling laws, to within error bars, and fall near the three dimensional Ising universality class.

The effect of secondary decays from hot initial fragments on the critical exponents has not been explicitly considered in this paper. In the SMM [36–39] such effects become significant above $E^*/A_0 = 7$ MeV/nucleon. Thus τ and γ, which are determined at lower excitation energies, will be unaffected in the SMM's fragment distributions. The exponent σ is determined by the multiplicities at which individual light fragment yields attain their peak values. As shown in Fig. 17(d), the lightest fragments peak at large multiplicities, corresponding to excitation energies for which secondary decay are important in the SMM. An SMM calculation [103] indicates that the value of σ from the SMM's fragment distribution was increased by about 70% due to this effect. However, it is unclear from that calculation that the effects of secondary decay are as great in the experimental data as they are in the SMM. The SMM calculation over predicts the yield of light fragments which could indicate that the SMM estimates of secondary decay are too severe. Corrections to the model independent quantities determined in this paper based on the SMM calculations are premature.
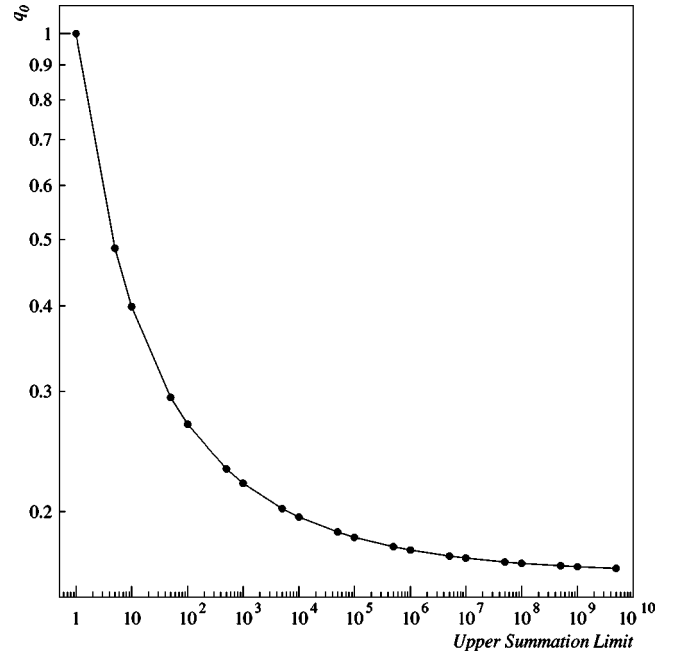
Although the multifragmentation data possess many of the gross and detailed characteristics that the percolation system does, it is not at all obvious why this should be the case. After all, real nuclei obey quantum mechanics, have varying binding energies per particle, and, most significantly, are charged. On the other hand, it is well known that near a critical point the details of the interaction become unimportant and only the dimensionality of the system and the dimension of the order parameter are important. As noted in the Introduction, the attractive nuclear force bears a similarity to a van der Waals force. However, the Coulomb force is a long range force and imposes a natural limit to the size of stable nuclei. Thus, it is not clear to what extent a finite charged system can exhibit critical behavior when the macroscopic system cannot exist. The exact role of the Coulomb force in physical systems undergoing a change of phase is currently of great interest [101,102] and is, at this point, an open question. The philosophy of this paper has been to make use of phase transition theory as it applies to uncharged systems. What results for the analysis of the gold multifragmentation data bears great similarity to the results of the same procedures applied to a system known to possess a critical point. It is tempting then to conclude that multifragmentation is related to critical behavior occurring in a finite nuclear system.

APPENDIX A: DISCUSSION OF POWER LAW IN RANDOM PARTITIONS

As a demonstration of the power of the sort of scaling analysis presented above it is shown that the random partitions follow a simple power law of $N_{A_f} \sim A_f^{-1}$. Figure 29 shows the scaled cluster distribution as a function of m from clusters with $A_f \geqslant 3$. The data nearly collapses to unity along the horizontal axis over the multiplicity range for $m > 5$. The deviations are due to the constraints of m and finite size. With a simple scaling analysis the underlying power law describing the cluster distribution becomes clear.

APPENDIX B: RIEMANN ζ FUNCTION SUMMATION

The value of q_0 used in this work based on the ζ function was generated with VAX FORTRAN code using double precision and letting the sum run from 1 to 10^6. The sum was terminated at this point in order to keep computing times within reason. For a value of $\tau = 2.18$ summing to 10^6 gives a value of q_0 that is within 10% of the value when the sum is terminated at 10^{10}, see Fig. 30. Increasing the upper limit of the summation in the ζ function causes no significant changes in the analysis presented in this work.

[1] B. Farizon *et al.*, Phys. Rev. Lett. **81**, 4108 (1998).

[2] A. Bonasera, Phys. World **12**, 20 (1999).

[3] E. E. B. Campbell *et al.*, contributions to *Proceedings of the Workshop on Nuclear Matter in Different Phases and Transitions*, Les Houches, France, 1998, edited by J. Blaizot *et al.* (Kluwer, Dordrecht, 1999).

[4] F. Kun and H. J. Herrmann, Phys. Rev. E **59**, 2623 (1999).

[5] J. E. Finn *et al.*, Phys. Rev. Lett. **49**, 1321 (1982).

[6] A. S. Hirsch *et al.*, Phys. Rev. C **29**, 508 (1984).

[7] M. E. Fisher, Physics (N.Y.) **3**, 255 (1967).

[8] M. E. Fisher, Rep. Prog. Phys. **30**, 615 (1969).

[9] D. Stauffer and C. S. Kiang, Adv. Colloid Interface Sci. **7**, 103 (1977).

[10] C. S. Kiang and D. Stauffer, Z. Phys. **235**, 130 (1970).

[11] R. W. Minich *et al.*, Phys. Lett. **118B**, 458 (1982).

[12] M. L. Gilkes *et al.*, Phys. Rev. Lett. **73**, 1590 (1994).

[13] J. B. Elliott *et al.*, Phys. Lett. B **381**, 24 (1996).

[14] J. B. Elliott *et al.*, Phys. Lett. B **418**, 35 (1998).

[15] X. Campi, J. Phys. A **19**, L917 (1986).

[16] X. Campi, Phys. Lett. B **208**, 351 (1988).

[17] X. Campi, Nucl. Phys. **A495**, 259 (1989).

[18] X. Campi and H. Krivine, Z. Phys. A **344**, 81 (1992).

[19] X. Campi and H. Krivine, Nucl. Phys. **A545**, 161 (1992).

[20] X. Campi and H. Krivine, contribution to the *International Workshop on Dynamical Features of Nuclei and Finite Fermi Systems* (World Scientific, Singapore, 1993).

[21] X. Campi and H. Krivine, contribution to the *International Workshop on Multi-Particle Correlations and Nuclear Reactions* (World Scientific, Singapore, 1994).

[22] X. Campi and H. Krivine, Nucl. Phys. **A620**, 46 (1997).

[23] H. Jaqaman, A. Z. Mekjian, and L. Zamick, Phys. Rev. C **27**, 2782 (1983).

[24] H. Jaqaman, A. Z. Mekjian, and L. Zamick, Phys. Rev. C **29**, 2067 (1984).

[25] A. L. Goodman, J. I. Kapusta, and A. Z. Mekjian, Phys. Rev. C **30**, 851 (1984).

[26] A. Z. Mekjain, Phys. Rev. Lett. **64**, 2125 (1990).

[27] A. Z. Mekjian, Phys. Rev. C **41**, 2103 (1990).

[28] S. L. Lee and A. Z. Mekjian, Phys. Rev. C **47**, 2266 (1993).

[29] K. C. Chase and A. Z. Mekjian, Phys. Rev. Lett. **75**, 4732 (1995).

[30] Y. Yariv and Z. Fraenkel, Phys. Rev. C **24**, 488 (1981).

[31] A. Gavron and Y. Yariv, Phys. Rev. C **41**, 2442 (1980).

[32] J. Cugnon, C. Volant, and S. Vuillier, Nucl. Phys. **A620**, 475 (1997).

[33] V. D. Toneev and K. K. Gudima, Nucl. Phys. **A400**, 173 (1983).

[34] P. Danielewicz, Phys. Rev. C **51**, 716 (1995).

[35] G. Peilert *et al.*, Rep. Prog. Phys. **57**, 533 (1994).

[36] J. P. Bondorf *et al.*, Nucl. Phys. **A443**, 321 (1985).

[37] J. P. Bondorf *et al.*, Nucl. Phys. **A444**, 460 (1985).

[38] J. P. Bondorf *et al.*, Phys. Rep. **257**, 133 (1995).

[39] A. S. Botvina *et al.*, Nucl. Phys. **A475**, 663 (1987).

[40] D. H. E. Gross, Rep. Prog. Phys. **53**, 605 (1990).

[41] D. H. E. Gross, Phys. Rep. **279**, 119 (1997).

[42] T. J. Schlagel and V. R. Pandharipande, Phys. Rev. C **36**, 162 (1987).

[43] J. Aichelin, Phys. Rep. **202**, 233 (1991).

[44] M. B. Belkacem *et al.*, Phys. Rev. C **52**, 271 (1995).

[45] S. Pratt, C. Montoya, and F. Ronning, Phys. Lett. B **349**, 261 (1995).

[46] V. Latora, M. Belkacem, and A. Bonasera, Phys. Rev. Lett. **73**, 1765 (1994).

[47] R. Donangelo and S. R. Souza, Phys. Rev. C **56**, 1504 (1997).

[48] C. J. Waddington and P. S. Freier, Phys. Rev. C **31**, 888 (1985).

[49] C. A. Ogilvie *et al.*, Phys. Rev. Lett. **67**, 1214 (1991).

[50] J. Hubele *et al.*, Z. Phys. A **340**, 263 (1991).

[51] P. Kreutz *et al.*, Nucl. Phys. **A556**, 672 (1993).

[52] L. G. Moretto *et al.* Phys. Rev. Lett. **71**, 3435 (1993).

[53] L. G. Moretto *et al.*, Phys. Rev. Lett. **74**, 1530 (1995).

[54] L. G. Moretto *et al.*, Phys. Rep. **287**, 249 (1997).

[55] L. Phair *et al.*, Phys. Rev. Lett. **79**, 3538 (1997).

[56] B. Elattari *et al.*, Nucl. Phys. **A560**, 603 (1993).

[57] C. Dorso *et al.*, Phys. Rev. C **60**, 034606 (1999).

[58] J. J. Binney *et al.*, *The Theory of Critical Phenomena*, 3rd ed. (Oxford University Press, Oxford, 1995).

[59] J. A. Hauger *et al.*, Phys. Rev. Lett. **77**, 235 (1996).

[60] J. A. Hauger *et al.*, Phys. Rev. C **57**, 764 (1998).

[61] D. Stauffer and A. Aharony, *Introduction to Percolation Theory*, 2nd ed. (Taylor and Francis, London, 1992).

[62] H. E. Stanley *et al.*, Physica A **266**, 5 (1999).

[63] D. Stauffer, Phys. Rep. **54**, 2 (1979).

[64] J. Hoshen *et al.*, J. Phys. A **12**, 1285 (1979).

[65] P. L. Leath, Phys. Rev. Lett. **36**, 921 (1976).

[66] P. L. Leath, Phys. Rev. B **14**, 5046 (1976).

[67] M. E. Fisher (private communication).

[68] H. Nakanishi and H. E. Stanley, Phys. Rev. B **22**, 2466 (1980).

[69] L. K. Nielsen *et al.*, Nature (London) **404**, 352 (2000).

[70] P. F. Mastinu *et al.*, Phys. Rev. Lett. **26**, 2646 (1996).

[71] J. B. Elliott *et al.*, Phys. Rev. C **49**, 3185 (1994).

[72] M. D'Agostino *et al.*, Nucl. Phys. **A650**, 329 (1999).

[73] A. D. Panagiotou *et al.*, Phys. Rev. Lett. **52**, 496 (1984).

[74] W. Bauer *et al.*, Phys. Lett. **150B**, 53 (1985).

[75] T. Li *et al.*, Phys. Rev. Lett. **70**, 1924 (1993).

[76] T. Li *et al.*, Phys. Rev. C **49**, 1630 (1994).

[77] S. Das Gupta and J. Pan, Phys. Rev. C **53**, 1319 (1996).

[78] C. Williams *et al.*, Phys. Rev. C **55**, R2132 (1997).

[79] A. Margolina *et al.*, J. Phys. A **17**, 1683 (1984).

[80] W. F. J. Müller (private communication).

[81] W. F. J. Müller, *Critical Phenomena and Collective Observables*, *Proceedings of the International Conference CRIS '96, Acicastello, Italy, 1996*, edited by S. Costa *et al.* (World Scientific, Singapore, 1996).

[82] W. H. Press, B. P. Flannery, S. A. Teukolsky, and W. T. Vettering, *Numerical Recipes* (Cambridge University Cambridge, 1986).

[83] J. B. Elliott *et al.*, Phys. Rev. C **55**, 1319 (1997).

[84] W. Bauer and W. A. Friedman, Phys. Rev. Lett. **75**, 767 (1995).

[85] M. L. Gilkes *et al.* Phys. Rev. Lett. **75**, 768 (1995).

[86] E. A. Guggenheim, J. Chem. Phys. **13**, 253 (1945).

[87] S. C. Greer, Phys. Rev. A **14**, 1770 (1976).

[88] J. Adler, M. Moshe, and V. Privman, Ann. Isr. Phys. Soc. **5**, 397 (1983).

[89] D. M. Saul, M. Wortis, and D. Jasnow, Phys. Rev. B **11**, 2571 (1975).

[90] H. Güttinger and D. S. Cannell, Phys. Rev. A **24**, 3188 (1981).

[91] M. W. Pestak and M. H. W. Chan, Phys. Rev. B **30**, 274 (1984).

[92] W. Bauer and A. Botvina, Phys. Rev. C **52**, R1760 (1995).

[93] J. B. Elliott *et al.*, Phys. Rev. C **55**, 544 (1997).

[94] M. E. Fisher and A. E. Ferdinand, Phys. Rev. Lett. **19**, 169 (1967).

[95] A. E. Ferdinand and M. E. Fisher, Phys. Rev. **185**, 832 (1969).

[96] M. E. Fisher and M. N. Barber, Phys. Rev. Lett. **28**, 1516 (1972).

[97] M. N. Barber, in *Phase Transitions and Critical Phenomena* edited by C. Domb and J. L. Lebowitz (Academic, New York, 1983), Vol. 8, p. 145.

[98] S. Albergo *et al.*, Nuovo Cimento A **89**, 1 (1985).

[99] H. R. Jaqaman *et al.*, Phys. Rev. C **29**, 2067 (1984).

[100] A. M. Ferrenberg and D. P. Landau, Phys. Rev. B **44**, 5081 (1991).

[101] R. P. Scharenberg *et al.*, submitted to Phys. Rev. C.

[102] M. E. Fisher, J. Stat. Phys. **75**, 1 (1994).

[103] Y. Levin, X. Li, and M. E. Fisher, Phys. Rev. Lett. **73**, 2716 (1994).